Finite Element Modelling of a Magma Chamber Surrounded by Country-Rock, with Particular Reference to the Groundwater Flow in Sections of Different Permeability

Thesis Submitted to

Rhodes University

in fulfillment of the requirements

for the degree of

Master of Science

CARMEN REMSING

December 2002

Abstract

This thesis presents results of two-dimensional finite element modelling of a magma chamber surrounded by country-rock containing a section of high permeability. The high permeability section in the country-rock simulates structure that is predominant in controlling the groundwater convection pattern and resulting mineral deposits. The models have analogies in nature: for instance the gold mines in the Massif Central of France, the Pogo mine in Alaska and the Pilgrim's Rest gold field in South Africa. This is a complicated coupled system involving fluid flow and heat transfer under extreme conditions. The magma in the chamber convects and as it cools the heat liberated causes convection in the groundwater contained in the surrounding country-rock. This convection in turn affects the rate of liberation of heat from the magma. The software used for the modelling, FLOTRAN, is the computational fluid dynamics component of the commercial ANSYS package.[1] The results obtained describe in detail the flow pattern in the magma chamber, the country-rock and high permeability section thereof. During the cooling of the magma chamber the groundwater convects more vigorously in the high permeability section than elsewhere, and a convection cell is seen forming within this region. This provides a mechanism for hydrothermal formation of valuable mineral deposits in the structure near a magma chamber. It is found that the relationship between the velocity of the flow in the cell and the temperature of the magma chamber is well represented by a first order linear differential equation, providing a simple understanding of this process.

[1] See Appendix A for a description of ANSYS.

Acknowledgements

I would like to thank my supervisors Professor Alan Rice and Dr Paul Nathanson for their constructive criticism and advice, and Professor John Moore for his assistance. I would also like to thank Professor Kotze and my colleagues at the Department of Mathematics for their encouragement and support. Thank you to all my friends especially Niki, Ashley, Ray and Anthony for their help. Many thanks to my family for being there for me all along.

Contents

List of Figures

List of Tables

Chapter 1

Introduction

South Africa's status as the world's preeminent gold producer is well known. Most of the gold is from quartz-pebble conglomerates in the Precambrian Witwatersrand Basin. The Pilgrim's Rest gold field covers an area of 600 km^2 and is centered near the town of Pilgrim's Rest. Discovered in 1872, the gold field has produced over 185 metric tons of gold with grades averaging from 6 to 40 g/ton, and an unknown, but probably comparable, amount of silver (Tyler and Tyler, 1996). As the placers were worked out, stratiform gold-silver ore bodies dominated the production. The understanding of these gold-silver ore bodies is still poor. Tyler and Tyler (1996) support the idea that the heat from intrusion of the Bushveld Igneous Complex (Rustenberg Layered Suite) to the west of Pilgrim's Rest, generated the auriferous hydrothermal solutions, and that its emplacement was the driving mechanism of thrust-fault deformation in the Pilgrim's Rest gold field (Figure 1.1).

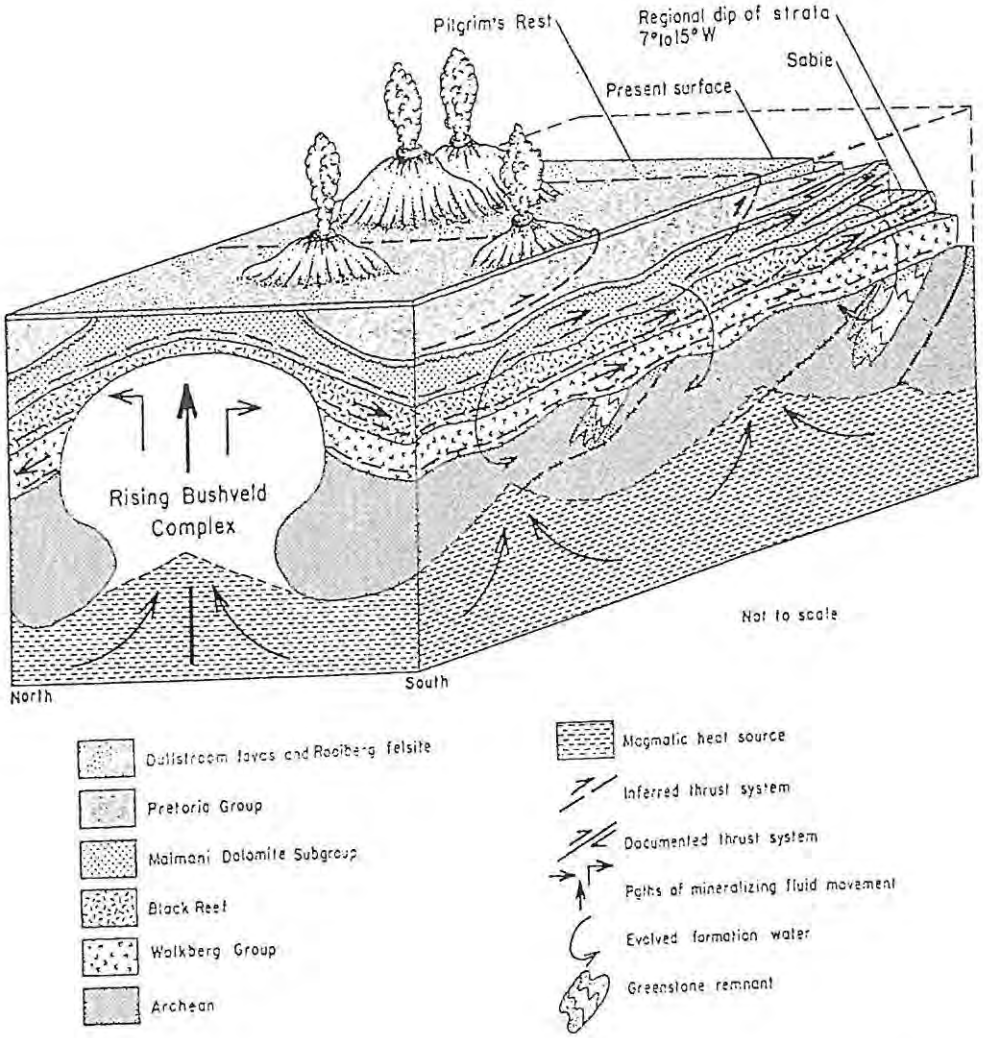

Figure 1.1: Emplacement model for stratabound ore bodies within the Pilgrim's Rest gold field. Modified from Tyler and Tyler (1996).

1.1 Aim of the thesis

This thesis is the fourth in a series from Rhodes University. The others are by Harrison (1998), Botha (1999), and Mbandezi (2001). Each concentrates on aspects of a program directed by Prof A Rice that is working towards a comprehensive system for modelling the deposition of minerals in the vicinity of magma chambers.

Here the models are two-dimensional and attention is focused on sections of high permeability in the country-rock surrounding a cooling magma chamber. These simulate geological structure in the country-rock. The specific aim is to characterize the flow patterns in a High Permeability Section (HPS), as these are expected to play a significant role in explaining the characteristics of the deposition of valuable minerals in systems such as Pilgrim's Rest gold field, the Massif Central gold mines in France or the Pogo gold mine in Alaska (Rice *et al.*, 2001).

While Harrison (1998) calculated the flow in country-rock surrounding a magma chamber, the same permeability was used throughout the country-rock, and special programming was added to the commercial package FLOTRAN to achieve these results. I however developed a new method for calculating flow patterns using standard options provided in the commercial software (viz., FLOTRAN in the ANSYS package) that requires no special programming.

1.2 Content of the thesis

Chapter 2 describes the magmatic fluid and its physical properties like density, viscosity, specific heat capacity and thermal conductivity. All these properties are necessary for modelling the magma flow. The numerical values used are those corresponding to a rhyolitic magma.

The country-rock surrounding the magma chamber is modelled as a porous medium with sections of different permeability. Chapter 2 also contains the numerical data and equations used to model the country-rock and groundwater.

The equations governing the flow of the magma and groundwater are presented in Chapter 3. The same equations are solved by FLOTRAN using numerical methods to model the fluid flow. These equations describe the physical laws of conservation: conservation of mass, momentum and energy. The unknowns which must be obtained simultaneously are the velocity, pressure and temperature. This chapter also contains a brief presentation of eulerian formulations of fluid dynamics problems.

Chapter 4 presents the numerical methods used to solve the governing equations for viscous flow and groundwater flow. Galerkin's method of weighted residuals is introduced in preparation to understanding the discretization methods used by FLOTRAN, which are presented in Chapter 5.

The theoretical presentation in these chapters is necessary to build up an exposition of the modelling process. The geometry and physical properties of the models are presented in Chapter 6.

The applied initial and boundary conditions and the experiments used to check the method employed are presented in Chapter 7.

The results in Chapter 8 provide a detailed description of the theoretical temperature and flow patterns for the cooling magma chamber and the convecting groundwater. Some preliminary results of the research were presented at the Exploration Geodynamics Conference, 19-24 August 2001, Western Australia (see Rice *et al.*, 2001). The results obtained show that there is a correlation between the maximum velocity in the HPS and the temperature variation of the cooling magma chamber. This correlation is described quite well by a simple linear differential equation. The solution to this differential equation gives the correct time at which the velocity of the flow in the HPS is at its maximum.

Chapter 9 presents a summary of 'open' and 'closed' model results and suggestions for further research topics involving the cooling of a magma chamber surrounded by country-rock of different permeability.

Appendix A presents an extract from the FLOTRAN Theoretical Manual to provide the reader with information about the ANSYS package.

Appendix B contains the steps followed in building up a typical model in ANSYS.

Appendix C is a glossary of geological terms.

Chapter 2

The intrusion-country-rock system

The initial conditions for the model begin immediately after the intrusive event which emplaces the magma chamber in the earth's crust which is when the magma is at its greatest temperature. Heat is allowed to flow from the magma chamber into the surrounding country-rock causing thermal convection of the ground water contained in it. The country rock is treated as a porous medium.

This chapter describes the relevant physical properties of the magmatic fluid and country-rock. The initial focus is on defining the viscosity, density, specific heat capacity and thermal conductivity of magma and determining their numerical values. Numerical values correspond to a rhyolitic type of magma. Thereafter the focus is shifted to the country-rock and groundwater, Darcy's Law, porosity, permeability. All the numerical values used are tabulated in Chapter 6.

2.1 Behaviour of magmatic melts in crustal intrusions

2.1.1 Magmatic fluids

Magma can be defined as 'a complete or partly molten natural substance, which, on cooling, solidifies as a crystalline or glassy igneous rock' (Williams and McBirney, 1979). The main component of magma is SiO_2. Magma usually contains crystals in suspension and volatiles in solution, and is capable of flowing under moderate stress (Williams and McBirney, 1979).

The physical properties of magma can be explained in terms of the properties of the silicon and oxygen ions which are the most abundant in igneous rocks. The molecular structure of magma is characterized by silica tetrahedra linked in a three dimensional network by oxygen atoms shared by two or more tetrahedra. Limited amounts of other cations can enter the molecular structure, and occupy positions between the tetrahedra. In this way, they modify the basic structural framework and alter its physical properties. The 'frame forming' atoms are Si and to a lesser degree Al. Ca, Mg, Fe, and Na are the 'framework modifiers'. The 'framework modifiers' can be accommodated up to 20 cation percent before the framework begins to break down into smaller geometric units. The original ratio of 1 to 2 Si atoms to O atoms changes to smaller Si / O ratios. When the 'framework modifiers' exceed 66 percent, each Si atom forms a separate tetrahedron which is not linked directly to another. Melts rich in 'framework modifiers' are named orthosilicates (Williams and McBirney, 1979).

Based on their SiO_2 content, most magma can be classified into three

major categories: mafic (or basaltic magma) with only about 50% SiO_2, andesite magma with a SiO_2 content between 50% and 70%, and felsic (or granitic) magma with a SiO_2 content of more than 70%. When a granitic magma cools inside the earth it forms a granite pluton or quartz porphyry dykes (Rogers and Hawkesworth, 2000).

2.1.2 Viscosity

Viscosity (μ) is usually defined as the ratio of shear stress to strain rate. The SI units for viscosity are $N \cdot m^{-2} \cdot s$. The shear stress in a magmatic fluid is often approximated with

$$\tau = \tau_0 + \mu \left(\frac{du}{dy} \right)^n \tag{2.1}$$

in which τ is the shear stress applied in the direction x parallel to the plane of flow, τ_0 is the minimum stress required to initiate permanent deformation, $\frac{du}{dy}$ is the velocity gradient normal to the plane of shear, and n is a constant less than or equal to 1 (McBirney and Murase, 1984). A fluid having no yield stress ($\tau_0 = 0$) and a direct linear relation between shear stress and the rate of strain ($n = 1$) is said to be *Newtonian*. Although, for convenience, magmas are commonly treated as Newtonian fluids, most are not. Below their liquidus, particularly when they are charged with phenocrysts, their rate of shear is not directly proportional to stress, i.e. $n < 1.0$ (McBirney and Murase, 1984).

The viscosity of silicate melts has three important characteristics. The first is that because the shear is proportional to the stress, the silicate melts exhibit Newtonian behaviour. The second is that the viscosity of silicate melts increases rapidly with decreasing temperature. Thirdly, the viscosity

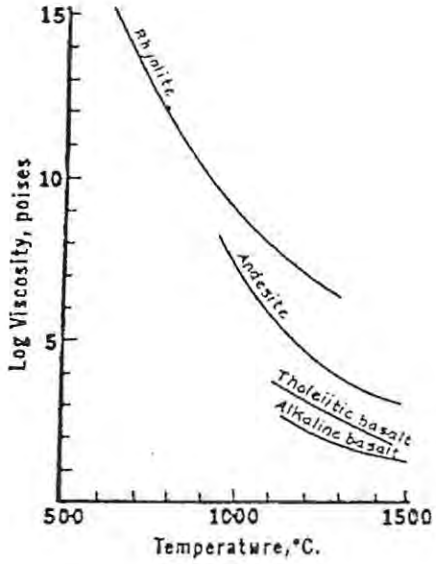

Figure 2.1: Viscosity of some igneous rocks as a function of temperature (Murase and McBirney, 1973).

of a liquid silicate melt depends strongly on melt composition. The most important component is SiO_2. The viscosity increases with increasing SiO_2 content in the melt. Low temperature rhyolitic melts have a viscosity that is as much as eight orders of magnitude (10^8) greater than that of high-temperature basaltic melts. This is due to a combination of the inverse dependence of viscosity on temperature and the positive covariation with the SiO_2 content (Wallace and Anderson, 2000).

Figure 2.1 shows the variation of viscosity with temperature for some common igneous rocks.

FLOTRAN allows viscosity formulations that simulate fluids with these properties. The equation used in FLOTRAN for the variation of viscosity

with temperature is :

$$\mu = \mu_n \exp\left\{ b_1 \left(\frac{1}{T} - \frac{1}{T_0} \right) + b_2 \left(\frac{1}{T} - \frac{1}{T_0} \right)^2 \right\} \tag{2.2}$$

where

$$\begin{aligned} T_0 &= \text{nominal temperature (K)} \\ \mu_n &= \text{nominal viscosity } (\mathrm{N \cdot m^{-2} \cdot s}) \\ T &= \text{temperature (K)} \\ b_1,\, b_2 &= \text{constants.} \end{aligned}$$

If it is necessary to model another type of magma, then the coefficients have to be recalculated with respect to nominal viscosities at nominal temperatures.

The nominal viscosity used here for magma of interest is $10^8 \mathrm{N \cdot m^{-2} \cdot s}$ at a nominal temperature of 1373 K (Murase and McBirney, 1973).

2.1.3 Density

Often, the equations of motion for fluids are simplified by considering that *density* is constant and uniform. However, the variation of density with temperature is crucial in natural convection. Pressure differences arising from these density variations drive the fluid into motion. A variation of density is crucial for heat and mass transfer. Density can be expressed as a function of pressure and temperature.

$$\rho = \rho(T, p) \tag{2.3}$$

The fluids modelled (magma and groundwater) have been taken to be incompressible, in that it is assumed that the pressure variations will not have

a significant effect on density, compared to thermal expansion or contraction. Hence density can be considered to be a function of temperature alone (Murase and McBirney, 1973)

$$\rho = \rho(T). \tag{2.4}$$

Figure 2.2 shows how the density of different igneous rocks varies with temperature. The shape of the graphs is comparable to that of half a parabola.

Williams and McBirney (1979) give the densities of some common igneous rocks at high temperatures. The densities range from about $2200\,\mathrm{kg \cdot m^{-3}}$ for rhyolite to $2800\,\mathrm{kg \cdot m^{-3}}$ for mafic basalts, and drop by a few percent between the crystalline and liquid states.

The density variation equation in FLOTRAN has a general formula dependent on temperature:

$$\rho(T) = \rho_n + c_1\,(T - T_0) + c_2\;(T - T_0)^2 \tag{2.5}$$

where

$$\begin{aligned} T_0 &= \text{nominal temperature (K)} \\ \rho_n &= \text{nominal density } \left(\mathrm{kg \cdot m^{-3}}\right) \\ c_1,\, c_2 &= \text{constants.} \end{aligned}$$

The nominal density used for magma is 2180 $\mathrm{kg \cdot m^{-3}}$ at the nominal temperature of 1373 K.

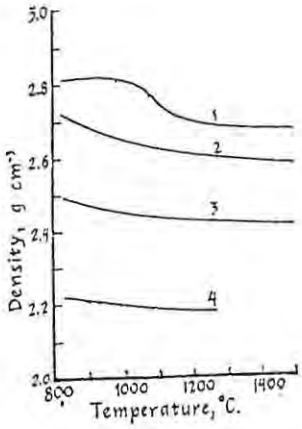

Figure 2.2: Densities of igneous rocks in the molten state as a function of temperature. 1 alkali basalt, 2 tholeiitic basalt, 3 andesite, 4 rhyolite (Murase and McBirney, 1973).

2.1.4 Thermal conductivity

Igneous rocks are very poor conductors of heat. The heat transfer mechanism has two components acting simultaneously: phonon conduction and radiative photon conduction. When the temperature increases, phonon conduction decreases and photon conduction increases. The two temperature effects tend to balance each other up to the melting range, but at high temperatures the conductivity of mafic rock declines at an increasing rate up to 1200° C. Over a limited temperature range the thermal conductivity of magma can be assumed constant (Williams and McBirney, 1979).

Figure 2.3 shows the variation of thermal conductivity with temperature. The thermal conductivity used for magma is 2 $\mathrm{J \cdot m^{-1} \cdot s^{-1} \cdot K^{-1}}$.

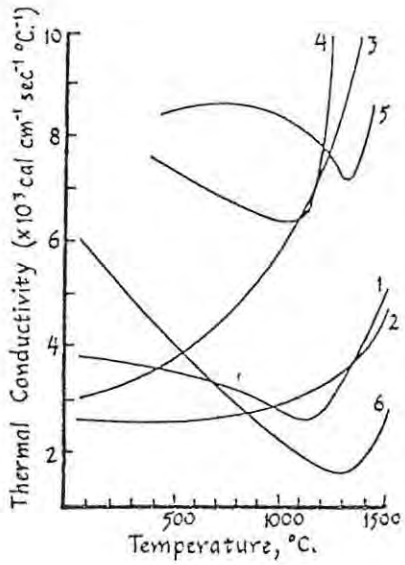

Figure 2.3: Thermal conductivity of igneous rocks as a function of temperature. 1 basalt, 2 andesite, 3 rhyolite, 4 dunite, 5 peridotite and 6 lunar basalt (Murase and McBirney, 1973).

2.1.5 Specific heat

There is a great contrast between the specific heat of magma or rocks and their heat of fusion or crystallization. The specific heat is usually much lower than the heat of fusion or crystallization. The specific heat at constant pressure is approximately 1200 $J \cdot kg^{-1} \cdot K^{-1}$ and the heat of fusion or crystallization is around 2590 $J \cdot kg^{-1} \cdot K^{-1}$ to 4100 $J \cdot kg^{-1} \cdot K^{-1}$ (Williams and McBirney, 1979).

Phase changes were not considered during the modelling, and therefore the specific heat value was kept constant. The value used for the magma is 1200 $J \cdot kg^{-1} \cdot K^{-1}$.

2.1.6 Coefficient calculations

Extreme care has to be taken in calculating the coefficients which describe the variation of density and viscosity with temperature, for both magmatic fluid as well as groundwater. The density and viscosity of magma increase with decreasing temperature as described by Equation (2.5) and Equation (2.2). The readings for the variation of viscosity and density with temperature for the magmatic fluid were taken from Figure 2.1 and Figure 2.2.

For calculating the coefficients c_1 and c_2, six readings for density at different temperatures were used. It is clear that we have an overdetermined system of six equations with two unknowns. It was therefore necessary to use a computer program (in this case Matlab 6.0.0.88 R12) to do a least squares best fit calculation of these coefficients. The same procedure was used to calculate the coefficients describing the variation of viscosity with temperature.

The coefficients calculated for the magma are: $b_1 = 11760.623$, $b_2 = -2615824.1$, $c_1 = -1.168748$, $c_2 = -138 \cdot 10^{-6}$.

The coefficients calculated for the groundwater are: $b_1 = -447.69$, $b_2 = 109327.08$, $c_1 = -0.45$, $c_2 = 0$.

2.2 Porous media and groundwater flow

For the purposes of this research a magma chamber completely surrounded by a country-rock that is treated as a porous medium was modelled. Bear (1972) defines a porous medium as 'a solid with holes'. If the holes or pores are interconnected with at least several continuous paths from one side of

the medium to the other and the pores have either a regular or random distribution over the entire solid, then the solid possesses permeability. A feature of the porous medium is that the various openings comprising the void are relatively narrow. The solid phase of a porous medium is called the matrix. The specific surface of the solid matrix is relatively high. The specific surface M of a porous medium is defined as the total interstitial surface area of the pores (A_s) per unit bulk volume (U_b) of the porous medium.

$$M = \frac{A_s}{U_b} \tag{2.6}$$

where $[M] = L^{-1}$ and L is length. Traditionally, the groundwater flow is modelled using *Darcy's Law* which predicts the specific discharge through an aquifer. Aquifers are underground storage reservoirs of water that are replenished naturally by precipitation and influant streams (Bear, 1972). Darcy's law is given by

$$\mathcal{U} = -K \frac{dh}{dl} \tag{2.7}$$

where $\mathcal{U}$ is the *specific discharge*, $\frac{dh}{dl}$ is the *hydraulic head or hydraulic gradient* and K is the *hydraulic conductivity*. Darcy's law is an empirically derived law based on the observation that discharge is proportional to the hydraulic gradient in the fluid. The specific discharge is the discharge per unit cross-sectional area normal to the direction of the flow. The units for specific discharge are $L \cdot T^{-1}$ where T is time.

Hydraulic conductivity K is a scalar (dimension $L \cdot T^{-1}$) which describes the ease with which a fluid is transported through a porous medium. It is, therefore, a coefficient that depends on both matrix and fluid properties. The relevant fluid properties are density ρ and viscosity μ.

The relevant solid matrix properties are mainly grain or pore size distribution, shape of grains or pore tortoisity, specific surface and porosity. *Porosity* is defined by Bear (1972) as the ratio of volume of the void space (U_v) to the bulk volume (U_b) of a porous medium. Porosity is dimensionless and is usually expressed in percent

$$n = \frac{U_v}{U_b}. \tag{2.8}$$

From a dimensional analysis it follows that we may express the hydraulic conductivity K as

$$K = \frac{\kappa \cdot g \cdot \rho}{\mu} \tag{2.9}$$

where g is the gravitational acceleration in $[\,\mathrm{m} \cdot \mathrm{s}^{-2}\,]$ and κ (dimension L^2) is called the *permeability* of the porous matrix and depends solely on the properties of the solid matrix.

The values used for permeability were taken from Table 2.1. The HPS was considered an 'oil rock' and the permeability was calculated as follows:

$$\begin{aligned} -\log_{10} \kappa[\mathrm{cm}^2] &= 9 \\ \kappa &= 10^{-9}[\mathrm{cm}^2] \\ \kappa &= 10^{-13}[\mathrm{m}^2] \end{aligned} \tag{2.10}$$

The rest of the country-rock was considered 'sandstone' and its permeability was taken again from Table 2.1:

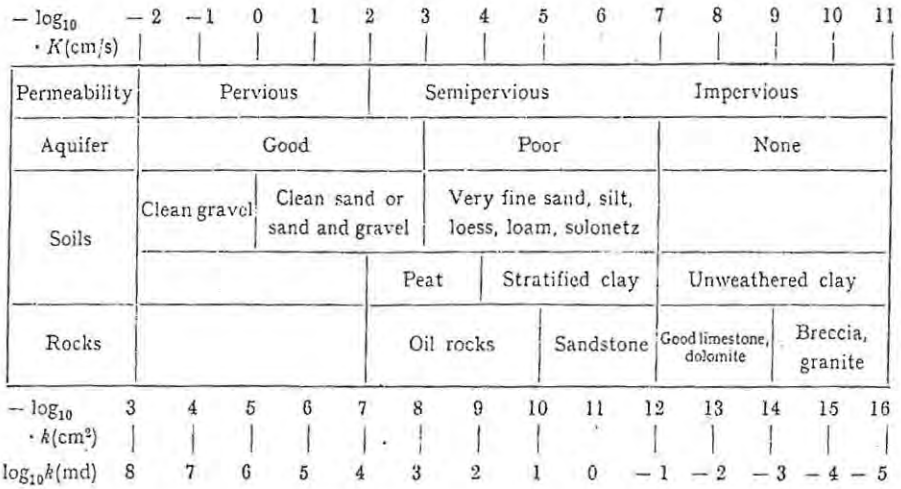

Table 2.1: Values for permeability and hydraulic conductivity for various geological formations (Bear, 1972).

$$-\log_{10}\kappa[\mathrm{cm}^2] = 11 \tag{2.11}$$

$$\kappa = 10^{-11}[\mathrm{cm}^2]$$

$$\kappa = 10^{-15}[\mathrm{m}^2]$$

Therefore the values assigned for the permeability of the HPS and the country-rock are $10^{-13}\mathrm{m}^2$ and $10^{-15}\mathrm{m}^2$.

This chapter has presented all the physical properties of the magmatic fluid and country-rock used in the study. Against this background attention can now be focused on the equations governing the flow of magma and groundwater.

Chapter 3

Equations governing magma and groundwater flow

This chapter presents the equations used to describe the flow of magmatic fluid as well as the flow of groundwater surrounding the magma chamber. A presentation of these equations is necessary in order to see why it is important that the physical properties of the fluids (viscosity, density, thermal conductivity and specific heat capacity) be well known. The same equations are solved by FLOTRAN to model the fluid flow.

These equations describe the physical laws of conservation: conservation of mass, conservation of momentum (or Newton's second law) and conservation of energy (or the first law of thermodynamics). The conservation of mass is described by the continuity equation, the conservation of momentum is described by the Navier-Stokes equations, and the conservation of energy is described by the energy equation (White, 1991). The unknowns which must be obtained simultaneously are the velocity $\vec{V}$, pressure p, and temperature T.

FLOTRAN uses the Galerkin weighted integral method, streamline upwinding method and a sequential solution algorithm for solving these equations. A detailed presentation of FLOTRAN algorithms can be found in the FLOTRAN Theoretical Manual (1992) which provides the theoretical foundation of FLOTRAN.

3.1 Eulerian formulation of motion

It is customary in fluid mechanics to choose the most convenient system of coordinates and to study only the velocity field as a function of position and time. This scheme of describing the flow at every fixed point as a function of time is called the eulerian formulation of motion (White, 1991).

The velocity vector $\vec{V}$ can be expressed as

$$\begin{aligned} \vec{V} &= \vec{V}(x,y,z,t) \\ &= \vec{i}u(x,y,z,t) + \vec{j}v(x,y,z,t) + \vec{k}w(x,y,z,t) \end{aligned} \tag{3.1}$$

Where $\vec{i}$, $\vec{j}$ and $\vec{k}$ are the unit vectors. Complete knowledge of the scalar variables u, v and w (as function of x, y, z and t) is often the solution to a fluid mechanics problem (White, 1991).

3.2 The continuity equation

In the eulerian system, the three laws of conservation (conservation of mass, momentum and energy) must use the substantial derivative

$$\frac{D}{Dt} = \frac{\partial}{\partial t} + \vec{V} \cdot \nabla \tag{3.2}$$

and the nabla operator

$$\nabla = \vec{i}\frac{\partial}{\partial x} + \vec{j}\frac{\partial}{\partial y} + \vec{k}\frac{\partial}{\partial z} \tag{3.3}$$

In eulerian terms, the law of conservation of mass (i.e. $m = \rho\mathcal{V}$) takes the form

$$\frac{D}{Dt}(\rho\mathcal{V}) = \rho\frac{D\mathcal{V}}{Dt} + \mathcal{V}\frac{D\rho}{Dt} = 0 \tag{3.4}$$

where m is the mass in $[\mathrm{kg}\cdot\mathrm{m}^{-2}]$, ρ is the density in $[\mathrm{kg}\cdot\mathrm{m}^{-3}]$ and $\mathcal{V}$ is the volume in $[\mathrm{m}^3]$ of a particle (White, 1991). But

$$\frac{1}{\mathcal{V}}\frac{D\mathcal{V}}{Dt} = \mathrm{div}\vec{V} \tag{3.5}$$

where $\mathrm{div}\vec{V}$ is the gradient operator

$$\mathrm{div}\vec{V} = \nabla\cdot\vec{V}$$

and hence

$$\frac{\partial\rho}{\partial t} + \mathrm{div}\rho\vec{V} = 0 \tag{3.6}$$

For incompressible flow, when ρ does not vary with time (i.e. $\frac{\partial\rho}{\partial t} = 0$), Equation (3.6) becomes

$$\mathrm{div}\vec{V} = 0. \tag{3.7}$$

3.3 The Navier-Stokes equations

In eulerian terms, the law of conservation of momentum for a newtonian viscous fluid flow is

$$\rho\frac{D\vec{V}}{Dt} = \rho\vec{g} - \nabla p + \mu\nabla^2\vec{V} \tag{3.8}$$

where $\vec{g}$ is the gravitational acceleration $[\,\mathrm{m}\cdot\mathrm{s}^{-2}\,]$ and p is pressure $[\,\mathrm{N}\cdot\mathrm{m}^{-2}\,]$ (White, 1991).

In scalar form, for an incompressible flow, we get

$$\begin{aligned}
\rho\frac{Du}{Dt} &= \rho g_x - \frac{\partial p}{\partial x} + \frac{\partial}{\partial x}2\mu\frac{\partial u}{\partial x} + \\
&\quad \frac{\partial}{\partial y}\left[\mu\left(\frac{\partial u}{\partial y}+\frac{\partial v}{\partial x}\right)\right] + \frac{\partial}{\partial z}\left[\mu\left(\frac{\partial w}{\partial x}+\frac{\partial w}{\partial z}\right)\right] \\
\rho\frac{Dv}{Dt} &= \rho g_y - \frac{\partial p}{\partial y} + \frac{\partial}{\partial x}\left[\mu\left(\frac{\partial v}{\partial x}+\frac{\partial u}{\partial y}\right)\right] + \\
&\quad \frac{\partial}{\partial y}2\mu\frac{\partial v}{\partial y} + \frac{\partial}{\partial z}\left[\mu\left(\frac{\partial v}{\partial z}+\frac{\partial w}{\partial y}\right)\right] \\
\rho\frac{Dw}{Dt} &= \rho g_z - \frac{\partial p}{\partial z} + \frac{\partial}{\partial x}\left[\mu\left(\frac{\partial w}{\partial x}+\frac{\partial u}{\partial z}\right)\right] + \frac{\partial}{\partial y}\left[\mu\left(\frac{\partial v}{\partial z}+\frac{\partial w}{\partial y}\right)\right] + \\
&\quad \frac{\partial}{\partial z}2\mu\frac{\partial w}{\partial z}
\end{aligned} \tag{3.9}$$

These are the Navier-Stokes equations for incompressible flow (White, 1991).

3.4 The energy equation

The eulerian form of the first law of thermodynamics is

$$\frac{DE_t}{Dt} = \frac{DQ}{Dt} + \frac{DW}{Dt} \tag{3.10}$$

where Q is the heat added to the system $[\mathrm{J}]$, J is joule, W is the work done on the system $[J]$ and E_t is the total energy of the system $[\mathrm{J}]$.

$$E_t = \rho\left(e + \frac{1}{2}V^2 - \vec{g}\cdot\vec{r}\right) \tag{3.11}$$

where e is the internal energy per unit mass $[\,\mathrm{J}\cdot\mathrm{k}g^{-1}\,]$, $\vec{g}$ is the gravitational acceleration $[\,\mathrm{m}\cdot\mathrm{s}^{-2}\,]$ and $\vec{r}$ is the displacement $[\,\mathrm{m}\,]$ (White, 1991). Equation

(3.11) becomes:

$$\frac{DE_t}{Dt} = \rho\left(\frac{De}{Dt} + V\frac{DV}{Dt} - \vec{g}\cdot\vec{V}\right). \tag{3.12}$$

By expressing the heat Q and the work W in terms of the fluid properties, for an incompressible flow, the energy equation is:

$$\rho\frac{Dh}{Dt} = \frac{Dp}{Dt} + \left(\frac{\partial q_x}{\partial x} + \frac{\partial q_y}{\partial y} + \frac{\partial q_z}{\partial z}\right) \tag{3.13}$$

where q_x, q_y and q_z are the cartesian components of heat transfer rate per unit area $[\mathrm{J}\cdot\mathrm{m}^{-2}]$

$$q_x = -k\frac{\partial T}{\partial x}$$

$$q_y = -k\frac{\partial T}{\partial y}$$

$$q_z = -k\frac{\partial T}{\partial z} \tag{3.14}$$

and k is the thermal conductivity and T is the temperature. h is the enthalpy [J],

$$h = e + \frac{p}{\rho}. \tag{3.15}$$

3.5 Summary of governing equations for a viscous fluid flow

The continuity equation, the Navier-Stokes equations and the energy equation can be written in a compact form for compressible flow, as follows:

3.5.1 Continuity equation

$$\mathrm{div}\vec{V} = 0 \tag{3.16}$$

3.5.2 Navier-Stokes equations

$$\rho\frac{D\vec{V}}{Dt} = \rho\cdot\vec{g} - \nabla\cdot p + \frac{\partial}{\partial x_j}\left[\mu\left(\frac{\partial v_i}{\partial x_j} + \frac{\partial v_j}{\partial x_i}\right)\right] \tag{3.17}$$

3.5.3 The energy equation

$$\rho\frac{Dh}{Dt} = \frac{Dp}{Dt} + \mathrm{div}(k\nabla T) \tag{3.18}$$

3.6 Porous medium flow

The flow of a fluid through a porous medium is an extremely complex phenomenon. The mathematical treatment of such a system in its complete complexity is practically impossible. It is therefore necessary to replace this complex system by a simplified one, where mathematical treatment can be applied. This is called 'the conceptual model' method. The results obtained analyzing the model, are in the form of mathematical relationships among various parameters of the investigated phenomenon. These results are then related to the real phenomenon (Bear, 1972).

3.7 A porous medium model

The most important characteristic of a porous medium is that the fluid flow is restricted to well defined channels. The velocity component of a fluid

particle (a fluid particle is an ensemble of molecules included in a certain volume), is at all times parallel to the walls of the solid matrix because of the proximity of these walls. There is no velocity component normal to the walls. The void space of the porous medium is composed of random channels or tubes of varying length and cross-section orientation, and junctions where the channels meet. The channels and the junctions are interconnected forming a spatial network. There is a clear difference between a junction and a channel. A channel has an elongated shape and a well defined axis. A junction has no definite direction in space. There is a uniform spatial distribution of channels and junctions through the solid matrix. The pattern of streamlines is fixed for any channel for the laminar flow considered in this analysis. There is no fixed pattern for the flow through a junction. The volume of a junction is much smaller than that of a channel. The solid matrix is rigid and noninteracting with the fluid. The fluid fills the void spaces completely (Bear, 1972).

3.8 Equation of motion for a fluid through a porous medium

The continuity equation, the Navier-Stokes equations and the energy equation are considered valid for any point in the fluid filling the void space of a porous medium.

The equation of motion of a fluid through a porous medium uses only average values for the different parameters which appear in these equations. The average values are taken over a *representative elementary volume* (REV). If P is the center of a sphere of volume ΔU_i, where $i = 1, 2, 3, \ldots$. For this

volume, the ratio n_i is defined as

$$n_i = n_i(\Delta U_i) = \frac{(\Delta U_v)_i}{\Delta U_i} \tag{3.19}$$

where $(\Delta U_v)_i$ is the volume of voids in the volume ΔU_i, then, as ΔU_i decreases, there is a volume ΔU_0, such as

$$n(P) = \lim_{\Delta U_i \to \Delta U_0} n_i[\Delta U_i(P)] = \lim_{\Delta U_i \to \Delta U_0} \frac{(\Delta U_v)_i}{\Delta U_i} \tag{3.20}$$

where $n(P)$ is the medium's volumetric porosity at point P. As $\Delta U_i \to 0$ n_i will be either 1 or 0, depending on P being a point of the void space or solid space. ΔU_0 is the representative elementary volume (REV) (Bear, 1972).

To obtain the equation of motion through a porous medium, the equation of conservation of momentum has to be rewritten in the view of the continuity equation, then write the velocity component at a point inside a channel. The viscous force per unit volume, R, $[\mathrm{N} \cdot \mathrm{m}^{-3}]$, is the force resisting the motion of the particle at a point inside the channel and is assumed to be of form

$$R = -(\mu/B)V \tag{3.21}$$

where μ is the viscosity, V is the velocity and B is the fluid conductance. The conduction, B is a function of the shape of the channel's cross-section and the location of the point in the channel (Bear, 1972).

The equation of motion becomes:

$$\mathcal{U}_i + \frac{B}{\nu} \cdot \frac{\partial \mathcal{U}_i}{\partial t} = -\frac{\kappa_{ij}}{\mu}\left(\frac{\partial p}{\partial x_j} + \rho g \frac{\partial z}{\partial x_j}\right) \tag{3.22}$$

where ν is the average kinematic viscosity $[m^2 \cdot s^{-1}]$ and $\mathcal{U}_i$ is the average discharge.

The second term on the left hand side of the equation expresses the local acceleration caused by the inertial forces. Usually these forces are much smaller than the viscous forces, so that the term can be dropped (Bear, 1979). Equation (3.22) then becomes:

$$\mathcal{U}_i = -\left(\frac{\kappa_{ij}}{\mu}\right)\left(\frac{\partial p}{\partial x_j} + \rho g \frac{\partial z}{\partial x_j}\right) \tag{3.23}$$

This equation is an extension of Darcy's law for flow in an anisotropic medium (Bear, 1972).

The equations presented in this chapter are necessary to model the magma and groundwater flow. The numerical methods used to solve such differential equations will be presented in Chapter 4. Chapter 5 will then consider the discretization methods used by FLOTRAN to solve the differential equations governing the magma and groundwater flow.

Chapter 4

Numerical methods used to solve differential equations

This chapter presents the numerical methods used to solve the governing equations for viscous fluid flow and groundwater flow presented in Chapter 3. Numerical methods are employed to solve differential equations when an exact solution is very difficult if not impossible to obtain because of the complexity of the differential equations and the geometry. The two main numerical methods are finite differences and the finite elements. The Galerkin method of weighted residuals is introduced in preparation to understanding the discretization methods used by FLOTRAN which will be presented in the next chapter. The finite element method, because of its flexibility is preferred for problems in which the boundaries are irregular or for problems in which the medium is heterogeneous or anisotropic (Wang and Anderson, 1982).

4.1 Finite differences method

The finite difference method replaces the differential equation by a difference equation. For example, if we want to solve an ordinary differential equation which is subjected to certain boundary conditions, say $y(0) = 0$ and $y(1) = 1$, then a grid has to be imposed on the problem domain. This involves deriving an appropriate difference equation and looking for solutions at the grid points, knowing that at $x = 0$ and $x = 1$ the solutions are fixed by the boundary conditions.

Iterative methods are usually used to solve the difference equations obtained. An advantage of iterative methods is that they tend to treat all the components equally and in this way, the error is distributed uniformly (DeVries, 1994). Another advantage of an iterative method is that the solution can be improved by iterating again (DeVries, 1994).

4.2 The finite element method

The finite element approach is another numerical method used to solve a partial differential equation, say in ξ. By applying the finite element method, the differential equation is replaced by a set of algebraic equations with a finite number of unknowns ξ_n at the finite number of nodal points. The nodal points are obtained by dividing the problem domain into intervals. The regions obtained form the so-called mesh. These unknowns, ξ_n, are the values of the function ξ at the nodal points. The nodes are used to form discrete volumes. These volumes are called finite elements. The discrete volumes can take many different shapes. For instance, four nodes will form a

tetrahedron. The selection of shapes depends on the geometry of the problem (Wang and Anderson, 1982).

The function ξ within each element is defined in terms of the nodal values by basis or interpolation functions. The function ξ is defined throughout the problem domain in a piecewise fashion over the individual elements. The definition of the function ξ throughout the problem domain in the finite element method permits the application of variational or weighted residual principles. A weighted residual principle is expressed directly in terms of the governing partial differential equations without to resort to a physical quantity.

Galerkin's method is based on the idea that a particular weighted average of the residual is forced to vanish. This way, the function ξ is obtained as the solution of a system of algebraic equations. The residual at each point in the problem domain is a measure of the degree to which the function ξ does not satisfy the governing equation.

An easy way to understand Galerkin's method is to apply it to Laplace's equation:

$$\frac{\partial^2 \xi}{\partial x^2} + \frac{\partial^2 \xi}{\partial y^2} = 0 \tag{4.1}$$

The first step is to define an approximate or trial solution $\tilde{\xi}(x, y)$. This function is expressed as a series summation where each term is a product of a nodal function ξ_L and an associated nodal basis function $N_L(x, y)$:

$$\tilde{\xi}(x, y) = \sum_{L=1}^{N} \xi_L \cdot N_L(x, y) \tag{4.2}$$

where $L = 1, ..., N$ is the nodal number, and N is the total number of nodes in the problem domain. The basis functions are unit vectors. This way, the

trial solution is built up as a linear combination of the basis functions (Wang and Anderson, 1982).

The second step requires a total of N conditions to determine the values of ξ_L. The N conditions in Galerkin's method are that the residuals of the governing equations weighted by each of the N functions be zero when integrated over the entire domain.

$$\int\int_D \left(\frac{\partial^2 \tilde{\xi}}{\partial x^2} + \frac{\partial^2 \tilde{\xi}}{\partial y^2} \right) N_L(x,y) dx dy = 0 \tag{4.3}$$

where D is the integration domain. The integration is done over the entire problem domain. The term

$$\frac{\partial^2 \tilde{\xi}}{\partial x^2} + \frac{\partial^2 \tilde{\xi}}{\partial y^2} \tag{4.4}$$

is the residual which is a measure of the extent to which $\tilde{\xi}(x,y)$ does not satisfy Laplace's equation. If $\tilde{\xi}(x,y)$ were the exact solution, then the residual would be zero everywhere. Galerkin's method requires that the residuals of the governing equations, weighted by each of the N basis functions, be zero when integrated over the entire problem domain.

The same restrictions as in Galerkin's method are those imposed by a variational principle, if it exists. Not all governing equations can be subjected to a variational principle. In such situations, Galerkin's method can be still applied (Wang and Anderson, 1982).

This step solves Equation (4.3). The basis functions $N_L(x,y)$ are usually defined in a piecewise continuous manner over the entire problem domain D. The first derivatives of $N_L(x,y)$ are also not necessarily continuous. Because

$\tilde{\xi}(x,y)$ is a linear combination of the basis functions $N_L(x,y)$, its second derivatives are not defined at step discontinuities of the first derivatives. By integrating by parts Equation (4.3), the order of the derivatives in the integrand is reduced by one. The integration by parts will be applied first to the one-dimensional form of Equation (4.3).

Let $u = N_L(x)$ and $v = \frac{d\tilde{\xi}}{dx}$. Then,

$$\int_a^b \frac{d^2\tilde{\xi}}{dx^2} N_L(x)dx = \frac{d\tilde{\xi}}{dx} N_L - \int_a^b \frac{d\tilde{\xi}}{dx} \cdot \frac{dN_L}{dx} dx \tag{4.5}$$

The two dimensional form of the generalized Equation (4.3) is

$$\int\int_D \left(\frac{\partial\tilde{\xi}}{\partial x^2} + \frac{\partial\tilde{\xi}}{\partial y^2} \right) N_L(x,y)dxdy = \tag{4.6}$$

$$-\int\int_D \left(\frac{\partial\tilde{\xi}}{\partial x}\frac{\partial N_L}{\partial x} + \frac{\partial\tilde{\xi}}{\partial y}\frac{\partial N_L}{\partial y} \right) dxdy + \int_\Gamma \left(\frac{\partial\tilde{\xi}}{\partial x} n_x + \frac{\partial\tilde{\xi}}{\partial y} n_y \right) N_L d\gamma$$

where Γ is the boundary of the domain D and γ is a generalized variable representing distance along the boundary. n_x, n_y are the components of a unit vector going normally outwards to Γ (Wang and Anderson, 1982).

A square problem domain is represented in Figure 4.1.

One can now consider a triangular element E in Figure 4.2

The first step in Galerkin's method is to define a trial solution $\tilde{\xi}(x,y)$ throughout the triangular element E by linearly interpolating the nodal values of ξ at the nodes surrounding the element. The nodes are in this case i, j, m. It can be written that

$$\tilde{\xi}^E(x,y) = a_0 + a_1 x + a_2 y \tag{4.7}$$

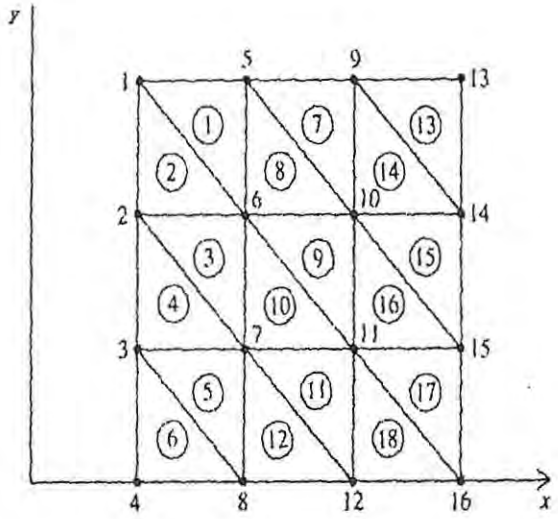

Figure 4.1: The mesh for a square problem domain. The circled numbers represent the elements. The nodes' numbers are not circled (Wang and Anderson, 1982).

where a_0, a_1 and a_2 are the coefficients that need to be determined. These coefficients can be determined from the three equations which require that the nodal values are obtained at the nodal coordinates:

$$\begin{aligned} \xi_i &= a_0 + a_1 x_i + a_2 y_i \\ \xi_j &= a_0 + a_1 x_j + a_2 y_j \\ \xi_m &= a_0 + a_1 x_m + a_2 y_m \end{aligned} \tag{4.8}$$

This system of three linear equations with three unknowns has to be solved for a_0, a_1 and a_2. The coefficients then have to be replaced in Equation (4.7). Equation (4.7) becomes:

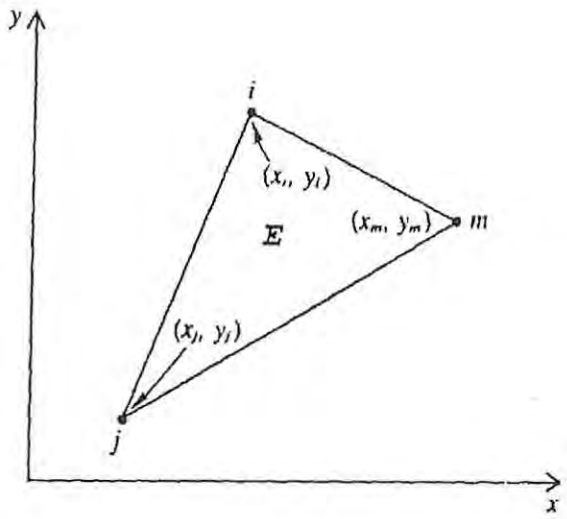

Figure 4.2: Triangular element, E. The nodes are labeled i, j, m (Wang and Anderson, 1982).

$$\tilde{\xi}^E = N_i^E(x,y)\xi_i + N_j^E(x,y)\xi_j + N_m^E(x,y)\xi_m \tag{4.9}$$

where

$$\begin{aligned} N_i^E(x,y) &= \frac{1}{2A^E}\left[(x_j y_m - x_m y_j) + (y_j - y_m)x + (x_m - x_j)y\right] \\ N_j^E(x,y) &= \frac{1}{2A^E}\left[(x_m y_i - x_i y_m) + (y_m - y_i)x + (x_i - x_m)y\right] \\ N_m^E(x,y) &= \frac{1}{2A^E}\left[(x_i y_i - x_j y_i) + (y_i - y_j)x + (x_j - x_i)y\right] \end{aligned} \tag{4.10}$$

where A^E is the area of the triangle ijm calculated using the coordinates at the corners. $N_i^E(x,y)$, $N_j^E(x,y)$ and $N_m^E(x,y)$ are the basis functions or the element interpolation functions. They are functions of spatial coordinates x

and y and they define $\tilde{\xi}(x,y)$ in element E in terms of the nodal values ξ_i, ξ_j and ξ_m. The same calculations are done for all the other nodes in the mesh.

This chapter has presented the numerical methods used to solve the differential equations governing the magma and groundwater flow. Chapter 5 will present the discretization methods used by FLOTRAN to solve these equations.

Chapter 5

Discretization methods used by FLOTRAN

This chapter shows briefly how FLOTRAN uses the numerical methods described in Chapter 4 to solve the governing equations describing the magma and groundwater flow. The continuity equation, the Navier-Stokes equations and the energy equation can all be written as a generalized transport equation:

$$\frac{\partial(\rho\Phi)}{\partial t}+\frac{\partial(\rho u\Phi)}{\partial x}+\frac{\partial(\rho v\Phi)}{\partial y}+\frac{\partial(\rho w\Phi)}{\partial z}=$$
$$\frac{\partial}{\partial x}\left(\Gamma_\Phi\frac{\partial\Phi}{\partial x}\right)+\frac{\partial}{\partial y}\left(\Gamma_\Phi\frac{\partial\Phi}{\partial y}\right)+\frac{\partial}{\partial z}\left(\Gamma_\Phi\frac{\partial\Phi}{\partial z}\right)+S_\Phi \qquad (5.1)$$

where $\frac{\partial(\rho\Phi)}{\partial t}$ represents the transient fluctuation of scalar quantity Φ in an infinitesimal control volume.

The next three terms, $\frac{\partial(\rho u\Phi)}{\partial x}+\frac{\partial(\rho v\Phi)}{\partial y}+\frac{\partial(\rho w\Phi)}{\partial z}$, represent the advection term. This is a term which describes the scalar Φ being transported in a known velocity field.

The term $\frac{\partial}{\partial x}\left(\Gamma_\Phi\frac{\partial\Phi}{\partial x}\right)+\frac{\partial}{\partial y}\left(\Gamma_\Phi\frac{\partial\Phi}{\partial y}\right)+\frac{\partial}{\partial z}\left(\Gamma_\Phi\frac{\partial\Phi}{\partial z}\right)$ represents the diffusion of

Φ with Γ_Φ as a generalized diffusion coefficient. Finally, S_Φ is a generalized source term.

This discretization process is used to derive the element matrices to obtain the matrix equation

$$\left(\left[M_e^{transient}\right] + \left[M_e^{advection}\right] + \left[M_e^{diffusion}\right]\right)\{Q_e\} = \{S_e^\Phi\} \tag{5.2}$$

where $\{Q_e\}$ is a column matrix containing the ξ_L values, where ξ_L is the value of function ξ at the Lth node.

5.1 The transient term

The transient term contribution to the element matrix is :

$$\left[M_e^{transient}\right] = \int W \left[\frac{\partial(\rho\Phi)}{\partial t}\right]^e d\forall^e \tag{5.3}$$

where $\forall^e$ shows that the integration is done for all elements e.

By applying a mass lumped approximation to the term in brackets we obtain a diagonal matrix whose elements are given by:

$$\int W \left[\frac{\partial(\rho\Phi)}{\partial t}\right]^e d\forall^e = \frac{\partial(\rho\Phi)_i}{\partial t} \int W_i \, d\forall^e \tag{5.4}$$

The $\frac{\partial(\rho\Phi)_i}{\partial t}$ term is approximated using a first order backward difference :

$$\frac{\partial(\rho\Phi)_i}{\partial t} = \frac{(\rho\Phi)_i^{K-2}}{2\Delta t} - \frac{4(\rho\Phi)_i^{K-1}}{2\Delta t} + \frac{3(\rho\Phi)_i^K}{2\Delta t} \tag{5.5}$$

where K corresponds to the current time level. The term at the current time level makes a contribution to the element coefficient matrix along with the advection and diffusion terms. The terms at the previous time steps make a contribution to the element source vector.

5.2 The advection terms

The advection terms are discretized by FLOTRAN using a monotone streamline upwind method. This method is based on the idea that pure advection transport is done along streamlines. Because advection means that a quantity is transported in a known velocity field, the advection terms can be expressed in terms of streamline velocities.

For an inviscid flow with no source terms, Equation (5.1) reduces to :

$$\frac{\partial(\rho u\Phi)}{\partial x}+\frac{\partial(\rho v\Phi)}{\partial y}+\frac{\partial(\rho w\Phi)}{\partial z}=0 \tag{5.6}$$

The expression represents pure advective transport of Φ in conservative form. In streamwise coordinates, Equation(5.6) can be rewritten as :

$$\frac{\partial(\rho u_s\Phi)}{\partial s}=0 \tag{5.7}$$

The streamline coordinate system is presented in Figure 5.1.

Because in pure advection transport all transfer occurs along streamlines, then when the advection term is expressed along a streamline, it is constant throughout the element and becomes:

$$\begin{aligned}\left[M_e^{advection}\right]=\int W\left[\frac{\partial(\rho u\Phi)}{\partial x}+\frac{\partial(\rho v\Phi)}{\partial y}+\frac{\partial(\rho w\Phi)}{\partial z}\right]^e d\forall^e=\\ \int W\left[\frac{\partial(\rho u_s\Phi)}{\partial s}\right]^e d\forall^e=\\ \left[\frac{\partial(\rho u_s\Phi)}{\partial s}\right]\int W\,d\forall^e\end{aligned} \tag{5.8}$$

FLOTRAN calculates $\frac{\partial(\rho u_s\Phi)}{\partial s}$ for an individual element. The first derivative which will give the gradient $\frac{\partial(\rho u_s\Phi)}{\partial s}$ is calculated using

$$\left[\frac{\partial(\rho u_s\Phi)}{dS}\right]^e=\frac{(\rho u_s\Phi)_{N1}-(\rho u_s\Phi)_{u_s}}{dS} \tag{5.9}$$

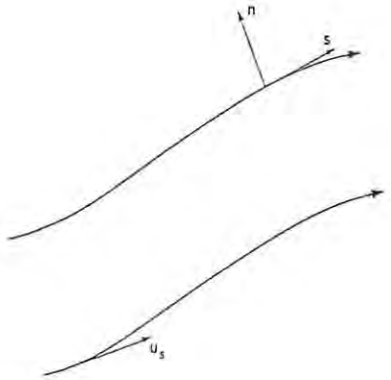

Figure 5.1: Streamline coordinate system (FLOTRAN theoretical manual, 1992)

where N_1 is the subscript for value at the downstream node, u_s is the subscript for value taken at the location at which the streamline through the downwind node enters the element, and ds is the distance from the upstream point to the downstream node. Figure 5.2 represents a tetrahedral element.

5.3 Diffusion term

To discretize the diffusion term in the governing equations, FLOTRAN uses Galerkin's method of weighted residuals. The term

$\frac{\partial}{\partial x}\left(\Gamma_\Phi \frac{\partial \Phi}{\partial x}\right) + \frac{\partial}{\partial y}\left(\Gamma_\Phi \frac{\partial \Phi}{\partial y}\right) + \frac{\partial}{\partial z}\left(\Gamma_\Phi \frac{\partial \Phi}{\partial z}\right)$ is integrated over the entire problem domain after being multiplied by a weighting function W, to obtain

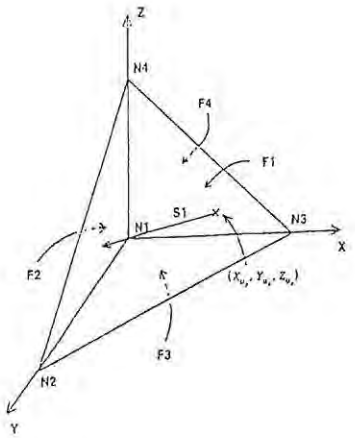

Figure 5.2: Streamline upwind approach for a tetrahedral element (FLOTRAN theoretical manual, 1992).

$$\int W \left[\frac{\partial}{\partial x} \left(\Gamma_\Phi \frac{\partial \Phi}{\partial x} \right) + \frac{\partial}{\partial y} \left(\Gamma_\Phi \frac{\partial \Phi}{\partial y} \right) + \frac{\partial}{\partial z} \left(\Gamma_\Phi \frac{\partial \Phi}{\partial z} \right) \right] d\forall^e = 0 \tag{5.10}$$

To transform the second order derivative terms in Equation (5.10) to first order derivative terms, one must integrate by parts. The equation obtained is:

$$\int \Gamma_\Phi \left[\frac{\partial W}{\partial x} \frac{\partial \Phi}{\partial x} + \frac{\partial W}{\partial y} \frac{\partial \Phi}{\partial y} + \frac{\partial W}{\partial z} \frac{\partial \Phi}{\partial z} \right] d\forall^e$$
$$- \int W \Gamma_\Phi \left[\frac{\partial \Phi}{\partial x} + \frac{\partial \Phi}{\partial y} + \frac{\partial \Phi}{\partial z} \right] dS^e = 0. \tag{5.11}$$

dS^e shows that the integration is done over the element surface S. When the derivative of Φ is replaced by the nodal values and the derivatives of

the weighting function then, by substituting $\Phi = \sum_{j=1}^{N} W_j \Phi_j$, and $\Gamma_\Phi = \sum_{j=1}^{N} W_j \Gamma_{\Phi_j}$, the nodal values will be removed from the integrals. N is the total number of nodes in the element.

The diffusion matrix obtained is:

$$[M_e^{diffusion}] = \int \sum_{i,j=1}^{N} W_i W_j d\forall^e \tag{5.12}$$

5.4 Source terms

Discretization of source terms consists of multiplying the source terms by the weighting function and integrating over all the elements.

The term obtained is:

$$S_\Phi = \int \sum_{i,j=1}^{N} W_i W_j S_{\Phi j} \forall^e \tag{5.13}$$

This chapter presented the discretization methods used by FLOTRAN to solve the governing equations for magma and groundwater flow. Chapter 6 will present the models and their dimensions as well as the physical properties of the magma and groundwater.

Chapter 6

The models: geometry and dimensions, physical properties and the mesh

The models presented in this chapter depict in two dimensions a cooling magma chamber surrounded by country-rock. This implies that the third dimension is considered infinite in extent. In the country-rock there is a horizontal section of much higher permeability than the rest of the rock. The country-rock and the high permeability section (HPS) are filled with groundwater. The geometry and dimensions of the magma chamber and country-rock are presented first. Although they are described in detail in Chapter 2, all the relevant physical properties are tabulated here for quick reference. The meshing procedure chosen for the models is also presented.

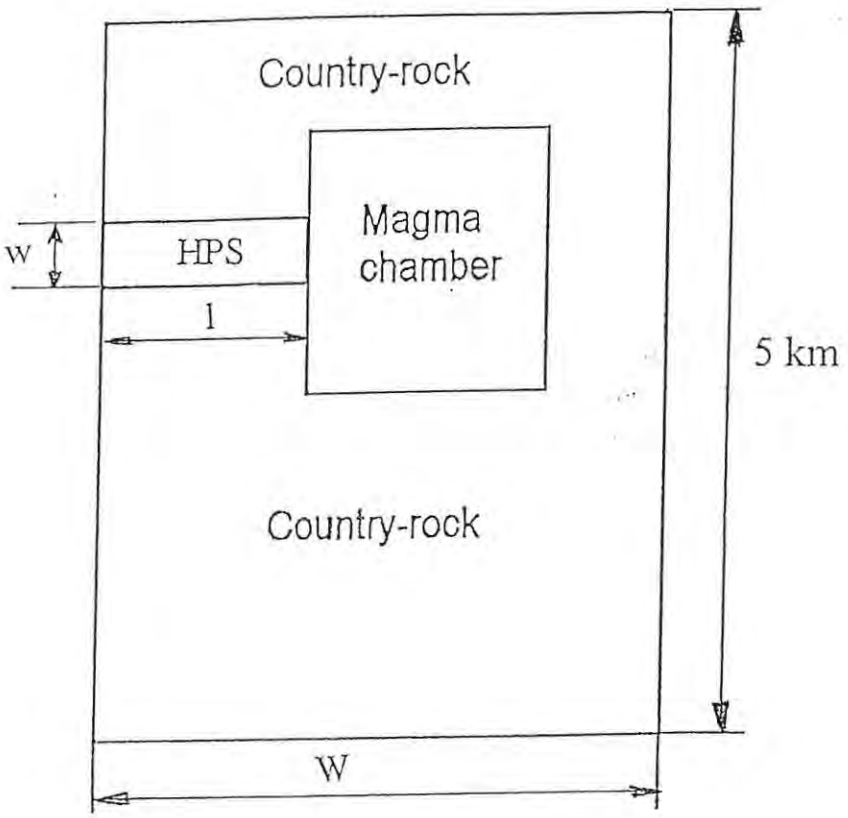

Figure 6.1: Schematic representation of the magma chamber and surrounding country-rock.

6.1 Geometry and dimensions

Figure 6.1 illustrates the magma chamber surrounded by the country-rock. The dimensions of the model are varied for study by using three different lengths and widths of the HPS.

The magma chamber is a square of 1 km × 1 km and is filled with rhyolitic magma. The dimensions of the magma chamber remain constant for all the models. The country-rock extends 1 km above the magma chamber, 1 km to the right and 3 km below the chamber. The HPS is half way up the side of the magma chamber. Table 6.1 presents all the dimensions which vary from

Model	Open or closed	Width and length of the HPS w × l	Width of the model W
A1	open	100 m × 1 km	3 km
A2	open	100 m × 7 km	9 km
A3	open	100 m × 10 km	12 km
B1	closed	100 m × 1 km	3 km
B2	closed	100 m × 7 km	9 km
B3	closed	100 m × 10 km	12 km
C1	open	500 m × 1 km	3 km
C2	open	500 m × 7 km	9 km
C3	open	500 m × 10 km	12 km
D1	closed	500 m × 1 km	3 km
D2	closed	500 m × 7 km	9 km
D3	closed	500 m × 10 km	12 km

Table 6.1: Dimensions for the width and length of the HPS, the width of the whole model.

one model to the other.

Two sets of models are designed: the first is referred to as an 'open' model, because the groundwater was allowed to leave the left and right hand side boundaries of the model. The second set of models is referred to as 'closed', because the groundwater was confined within the boundaries of the model. In the discussion that follows, the term 'open' or 'closed' will be used to differentiate these two sets of models.

Physical property	Symbol	Numerical value	Units
Density	ρ	2180	$kg \cdot m^{-3}$
Specific heat	c_v	1200	$J \cdot kg^{-1} \cdot K^{-1}$
Thermal conductivity	k	2	$J \cdot m^{-1}s^{-1} \cdot K^{-1}$

Table 6.2: The physical properties of the 'solid' section.

6.2 Physical properties of the fluids modelled

In all models, the magma chamber was surrounded by a very thin (1 m) artificial 'solid' section to separate the liquid magma from the groundwater. The physical properties of the 'solid' section are presented in Table 6.2 (as presented in Chapter 2). These values are the same as those for the magma with the density constant at nominal value. Some calculations were done with different wall thickness to check the influence the 'solid' wall has on the model's behaviour. The influence of the separating wall was negligible from the heat transfer point of view.

Table 6.3 lists the physical properties of the magmatic fluid used for the modelling. These properties remain are the same for all the models. The values used are based on the properties of magmatic melts and groundwater flow presented in Chapter 2.

The physical properties of the groundwater filling the country-rock are presented in Table 6.4. These properties were obtained from the Handbook of Tables for Applied Engineering Science (Boltz and Tuve, 1973).

Physical property	Nominal values and coefficients	Numerical value
Density (ρ)	Nominal value (ρ_n)	$2180\ \mathrm{kg \cdot m^{-3}}$
	Linear coefficient (c_1)	-1.168748
	Quadratic coefficient (c_2)	$-138 \cdot 10^{-6}$
Viscosity (μ)	Nominal value (μ_n)	$1 \cdot 10^{8}\mathrm{N \cdot s \cdot m^{-2}}$
	Linear coefficient (b_1)	11760.623
	Quadratic coefficient (b_2)	-2615824.1
Thermal conductivity (k)	constant	$2\ \mathrm{J \cdot m^{-1} \cdot s^{-1} \cdot K^{-1}}$
Specific heat (c_v)	constant	$1200\ \mathrm{J \cdot kg^{-1} \cdot K^{-1}}$

Table 6.3: The physical properties of the magmatic fluid used

6.3 The mesh

The mesh is an important part of the modelling process. The shape and number of elements chosen have an influence on the final result. Therefore, at the outset, the mesh can be coarse in order to speed up the computing time. Once relevant results are obtained, the number of elements should be increased to see how the new results differ from those obtained previously. If the difference is less than 10%, it is not advisable to work with a finer mesh because the physical parameters are not that well known to incur the considerable increase in computing time. A mesh with 10 divisions/length was chosen initially. This was then increased to 30 divisions/length. This was then used throughout all the models. Figure 6.2 shows the mesh used for modelling.

This chapter presented the geometry of the models, their dimensions and

Physical property	Nominal values and coefficients	Numerical value
Density (ρ)	Nominal value (ρ_n)	$1045\ \mathrm{kg \cdot m^{-3}}$
	Linear coefficient (c_1)	-.045
	Quadratic coefficient (c_2)	0
Viscosity (μ)	Nominal value (μ_n)	$12.11 \cdot 10^{-6}\mathrm{N \cdot s \cdot m^{-2}}$
	Linear coefficient (b_1)	-447.69
	Quadratic coefficient (b_2)	109327.08
Thermal conductivity (k)	constant	$2\ \mathrm{J \cdot m^{-1} \cdot s^{-1} \cdot K^{-1}}$
Specific heat (c_v)	constant	$4342\ \mathrm{J \cdot kg^{-1} \cdot K^{-1}}$
Permeability of country-rock (K_1)	constant	$1 \cdot 10^{-15}\mathrm{m^{-2}}$
Permeability of the HPS (K_2)	constant	$1 \cdot 10^{-13}\mathrm{m^{-2}}$

Table 6.4: The physical properties of the groundwater

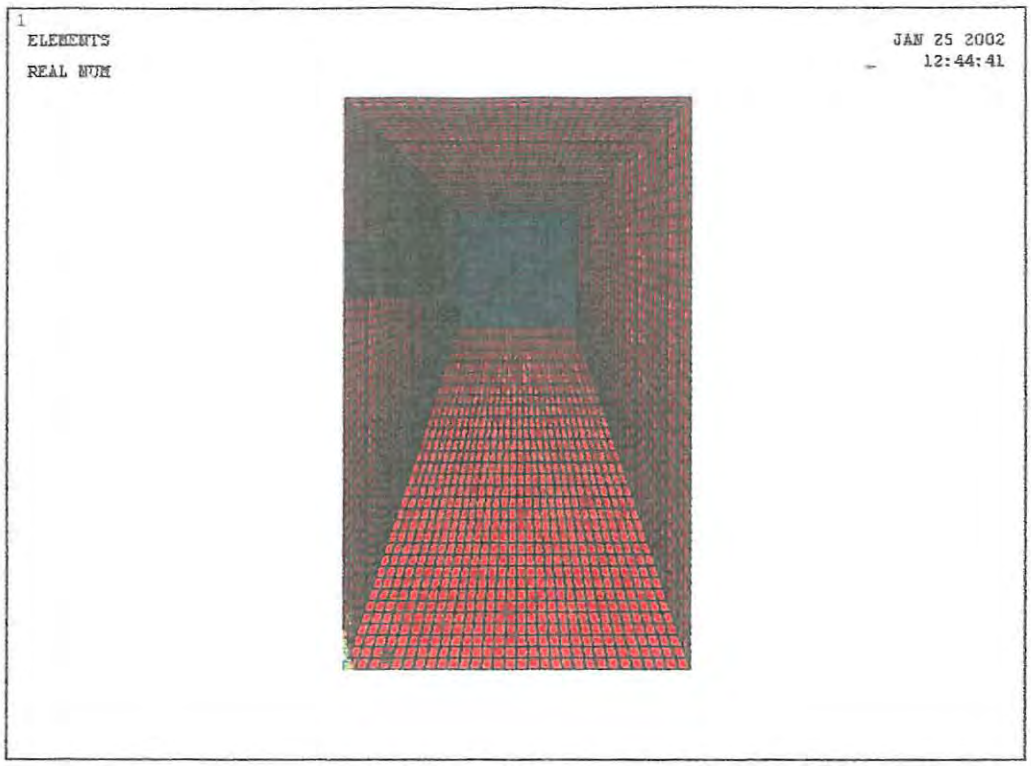

Figure 6.2: The 30 divisions/length mesh

the physical properties used to model the magma and groundwater flow. It also explained the mesh used in the modelling process. Chapter 7 presents the preliminary experiments performed using to verify the calculations.

Chapter 7

Preliminary numerical experiments and calculations

This chapter presents experiments devised to check the method employed to obtain the final results. These experiments were necessary because the method is a new one based on the 'Heat Exchanger' example provided by the ANSYS support group. The 'Heat Exchanger' example models the heat flow between two different fluids at different temperatures separated by a very thin solid wall using the Multiple Species option in the Computational Fluids Dynamics (CFD) package (details of the Multiple Species option are given in Appendix A).

The 'Heat Exchanger' example presents a close resemblance to the very hot magmatic fluid in the magma chamber and the relatively cold groundwater surrounding it, as the thin solid wall represents the quenched magma on the original wall of the volume holding the magma.

7.1 The experiments

Two different methods were applied to the same models. The first method is the one used in all previous magma chamber calculations (Harrison 1998, Botha 1999 and Mbandezi 2001). It uses the Single species option provided in the ANSYS package. The second method is the new one that uses the Multiple Species option.

The first method could only be used on the magma chamber cooling without groundwater flow, because Harrison's (1998) additional programming did not work on the later versions of ANSYS. The best that could be done with groundwater flow was to compare results directly with those published by Harrison (1998). The dimensions of the magma chamber were held constant at 1 km $\times$ 1 km for all the models. Temperature and velocity readings were taken at the same time intervals in each pair of calculations so that direct comparisons could be made.

7.1.1 Model 1

The first model involved the cooling of a magma chamber from an initial temperature of 1273 K over a period of 4000 years. Very low temperature (273 K) boundary conditions were applied along the sides of the magma chamber. The temperature and velocity readings at the same time intervals were identical for the two methods applied. Figure 7.1 shows the temperature profile of the cooling magma chamber after 2500 years. All temperatures are given in Kelvin.

Figure 7.2 represents the vector velocity profile of the same cooling magma chamber after 2500 years. The velocities are given in m/s. Note that the length of

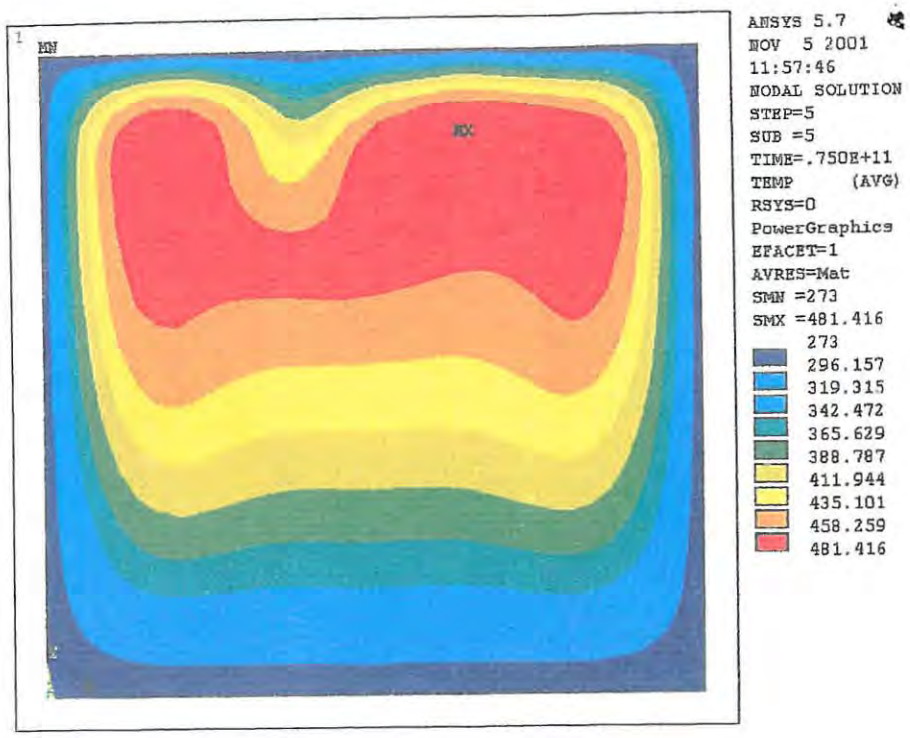

Figure 7.1: Temperature profile of a cooling magma chamber.

the vectors shown are directly proportional to the magnitude of the velocities, and the colour coding is also used to illustrate the magnitude of the velocities. Because both methods gave the same readings, only one set of pictures is presented.

7.1.2 Model 2

The second model tested was slightly more complicated. It contained the same magma chamber as before, but this time it was surrounded by a 3 km $\times$ 3 km country-rock. The temperature boundary conditions were 273 K at the top of the model and 398 K at the bottom. These temperatures were chosen to replicate the geothermal gradient of 25 K/km. The initial temperature of the magma chamber was 1273 K and the cooling process was monitored over 4000 years. The temperature and velocity readings were taken at the same time intervals and were the same for the two methods applied. Figure 7.3 and Figure 7.4 show the temperature and velocity profiles of the cooling magma chamber after 3000 years.

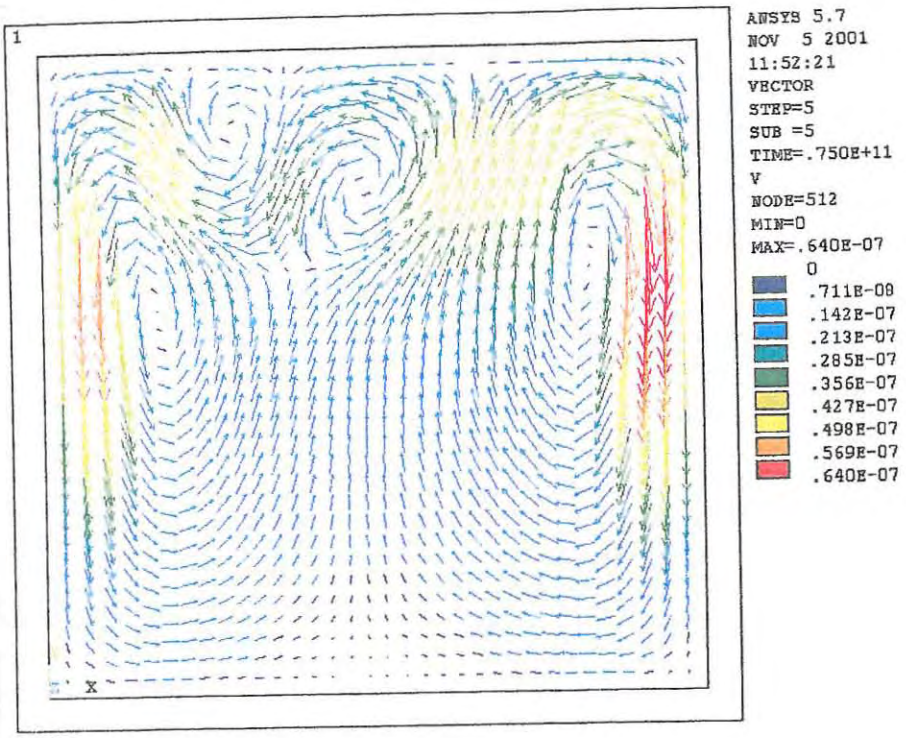

Figure 7.2: Velocity profile of a cooling magma chamber.

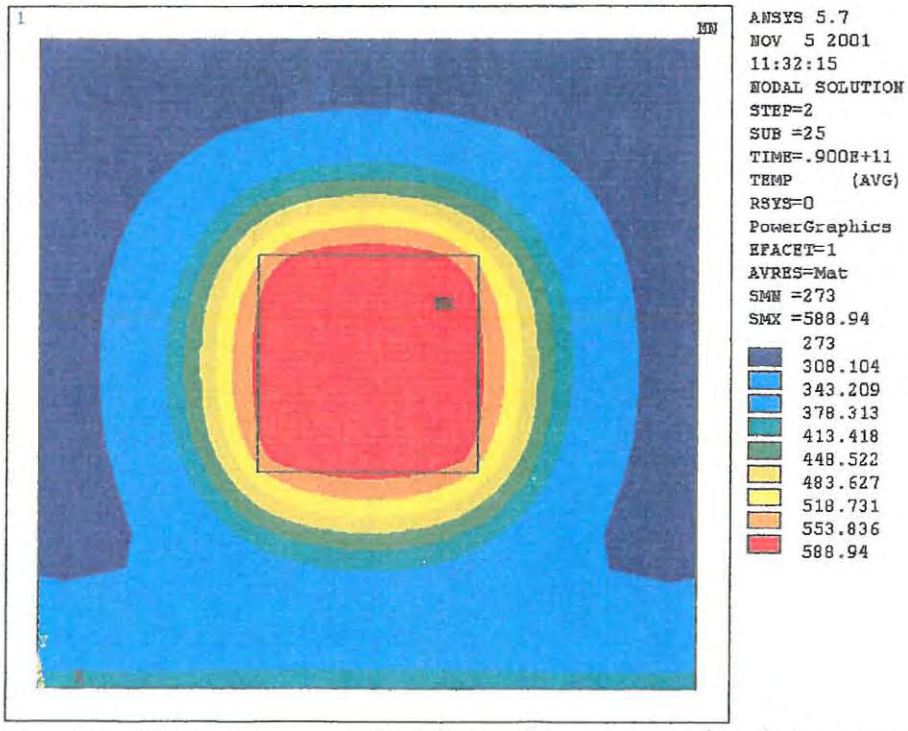

Figure 7.3: Temperature profile of a cooling magma chamber surrounded by country-rock.

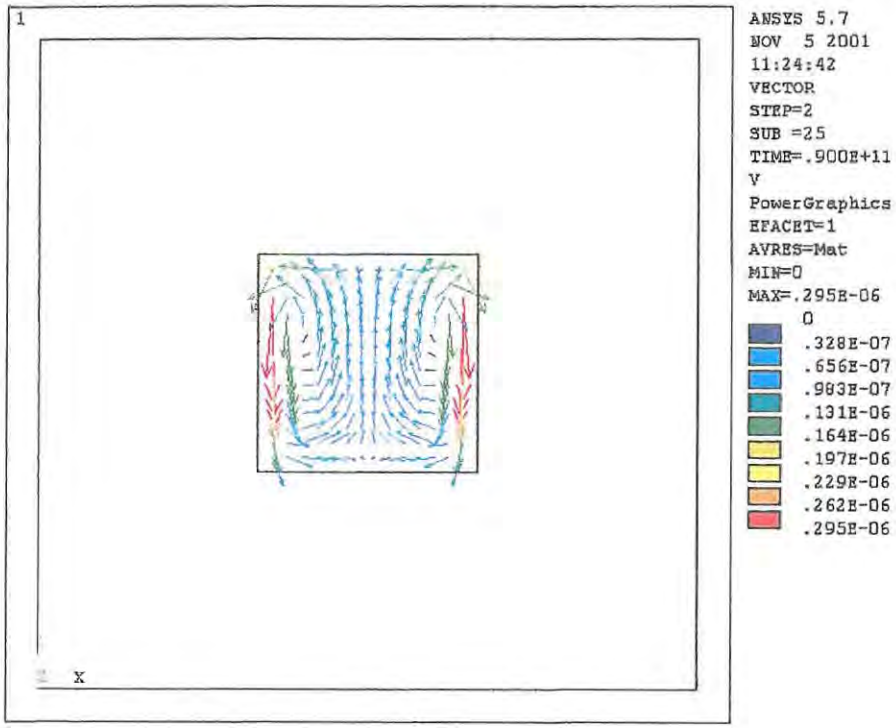

Figure 7.4: Velocity profile of a cooling magma chamber surrounded by country-rock.

From this point on, it was not possible to test the two methods in parallel any further because the usual ANSYS approach which only employs a single species is not applicable in modelling two different fluids at the same time. Nevertheless, the outcome of the experiments suggested that the Multiple Species method is reliable and can be used successfully for the models of interest.

7.2 Initial and boundary conditions applied in the models

All models are of a magma chamber surrounded by country-rock filled with groundwater. The magma chamber is treated as if the magma is injected in a single event over an infinitesimal time period (on a geological scale) into the

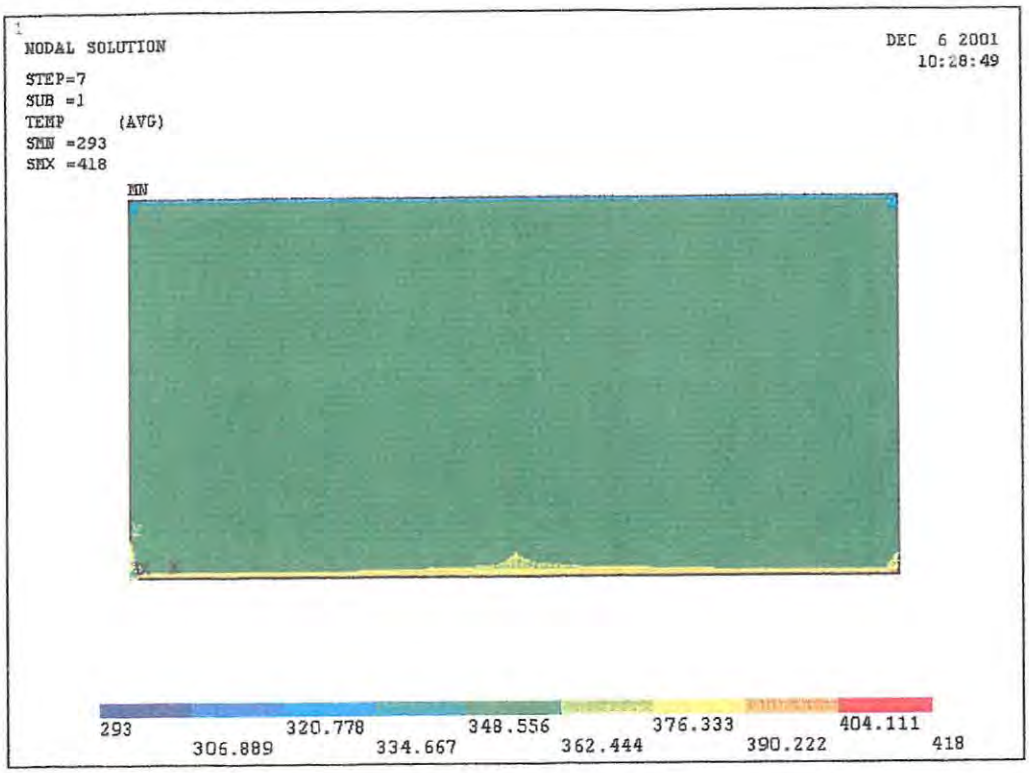

Figure 7.5: Temperature profile of the country-rock filled with groundwater. The only significant changes in temperature occur near the top and bottom surfaces,i.e., the fluid overwhelmed the geothermal gradient.

crust from the mantle and then proceeds to cool and solidify. The country-rock and the groundwater in it are subjected to the geothermal gradient. It was therefore of interest to calculate the temperature and velocity distributions of the water in a country-rock filled with groundwater under the geothermal gradient but without a magma chamber. Figures 7.5 and 7.6 represent the temperature and velocity profiles of the groundwater once a dynamic thermal equilibrium was reached. The temperature is 293 K at the top of the model and 418 K at the bottom using a geothermal temperature gradient of 25 K/km. As before, the temperatures and velocities are given in K and m/s respectively. These results were considered as initial conditions for the Models A, B, C and D. Table 7.1 and 7.2 give the initial and boundary conditions used in all the models for the magma chamber and the country-rock.

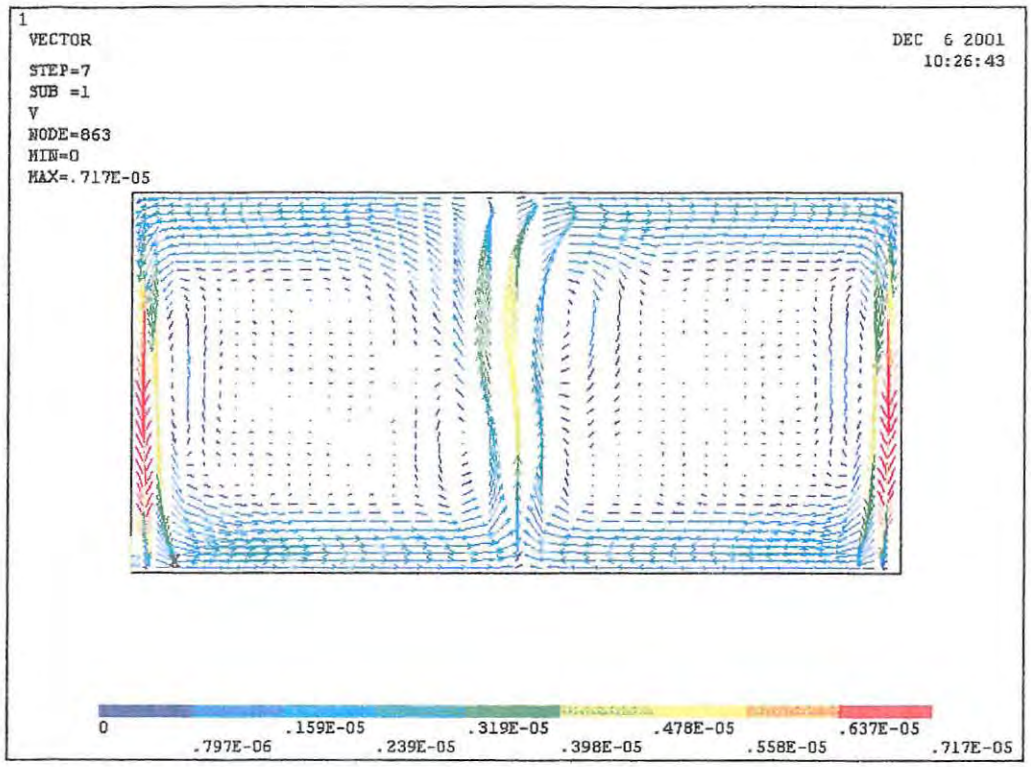

Figure 7.6: Velocity profile of the convecting groundwater under the geothermal gradient.

Initial conditions	Boundary conditions
T = 1273K	$v_x = v_y = 0$
at all nodes	at all exterior nodes

Table 7.1: Initial and boundary conditions for the magma chamber. T is temperature in K and v_x and v_y represent velocity in x and y direction.

Initial conditions	Boundary conditions
T = 348K on all nodes	$v_x = v_y = 0$ on all exterior nodes for models B and D
	$v_x = v_y = 0$ on top and bottom nodes for models A and C
	T = 293K for top nodes T = 418K for bottom nodes

Table 7.2: The initial and boundary conditions for the country-rock. T is temperature in K and v_x and v_y represent velocity in x and y direction.

This chapter presented the models and experiments conducted to verify the method employed for modelling the magma chamber surrounded by the country-rock. The results of the calculations with the HPS in the country-rock are presented in Chapter 8 together with discussions thereof and conclusions.

Chapter 8

Results

This chapter presents the main results. These are obtained for the 12 models A1 to D3 specified in Chapter 6. The cooling magma chamber is surrounded by country-rock with a higher permeability section (HPS) of different dimensions connected to one side of the chamber as shown in Figure 6.1. The country-rock has variable permeability and is filled with groundwater. The temperature and velocity readings are taken at 1000 year intervals. The reason for choosing this time interval is that there are no significant changes in the readings for smaller time intervals. The diagrams presented are only the most significant ones describing the convection of the groundwater and the cooling of the magma chamber. There are no major differences between the 'open' and 'closed' models with respect to the temperature and velocity magnitudes. The biggest difference is the fact that for the 'closed' model a convection cell forms in the HPS. The temperature-time graphs and the velocity-time graphs presented will show how the magnitudes vary with time. There is a correlation between how the magnitude of the velocities in the HPS varies with the temperature of the adjacent magma chamber. To investigate this correlation, another numerical experiment was

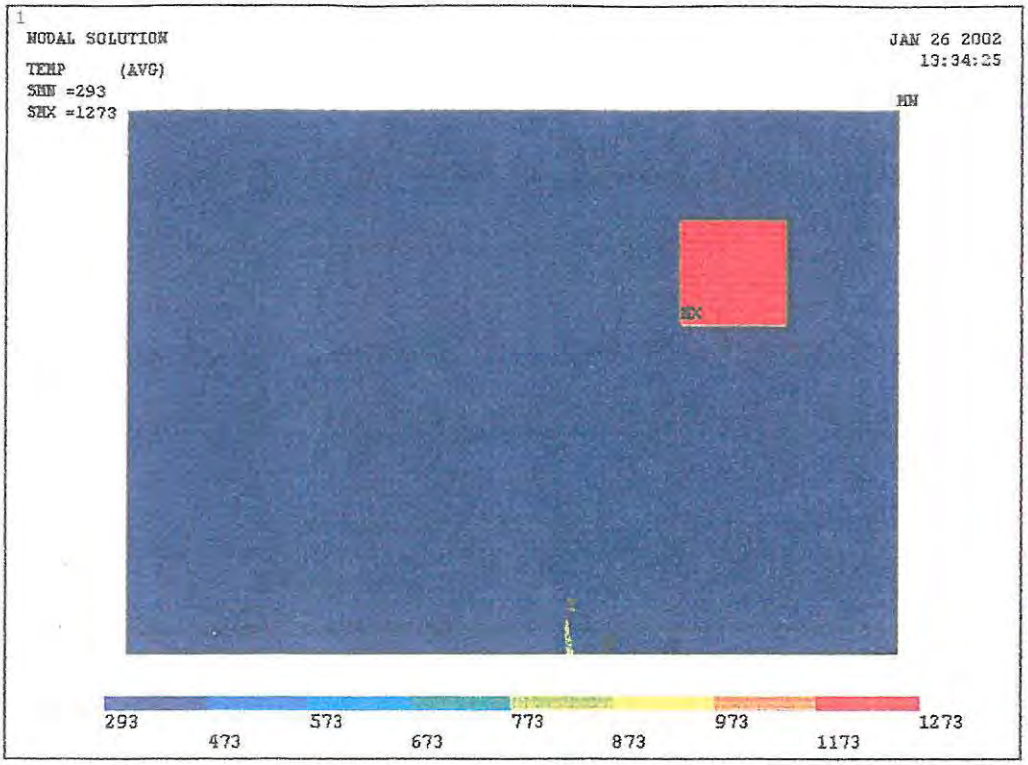

Figure 8.1: Initial temperature profile for Model C2.

set up. It is found that the correlation is described quite well by a first order linear differential equation providing a simple intuitive understanding of the effect of the magma temperature on the velocities in the HPS.

8.1 The 'open' model results

8.1.1 The magma chamber

The calculation of magma chamber cooling was carried over a period of 5000 years. For all the models, the cooling curve looks similar. Figures 8.1 and 8.2 show the initial temperature of the model and the temperature profile after 2000 years. Details within the different regions are lost because of the large difference between the temperatures of the magma and the country-rock.

The cooling graphs of the HPS in Models A and C (the 'open' models - see Table 6.1) are presented in Figures 8.3 and 8.4.

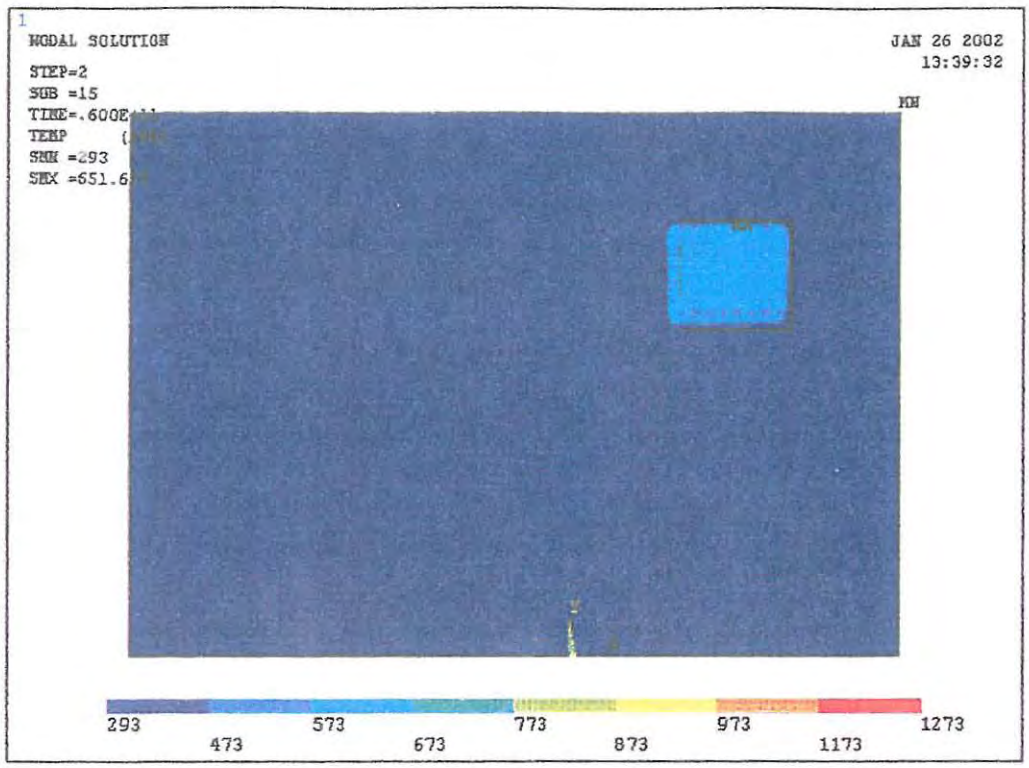

Figure 8.2: Temperature profile after 2000 years for Model C2 (see Table 6.1).

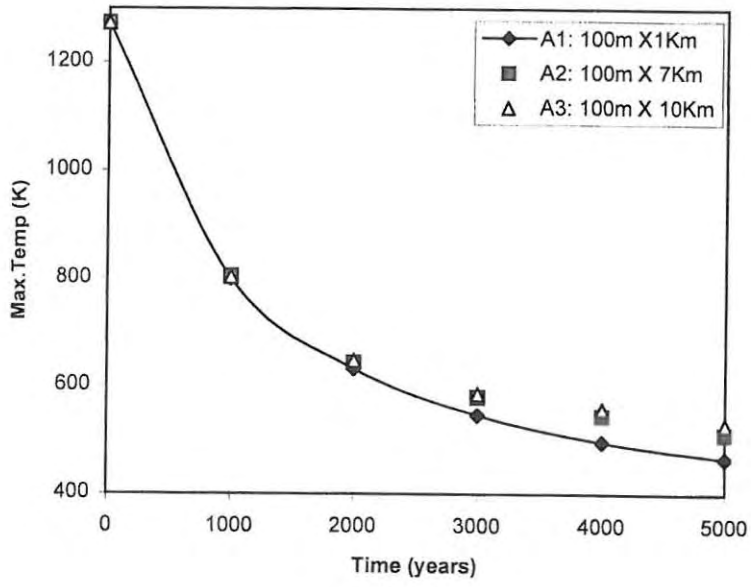

Figure 8.3: Maximum temperature vs time graph for Model A.

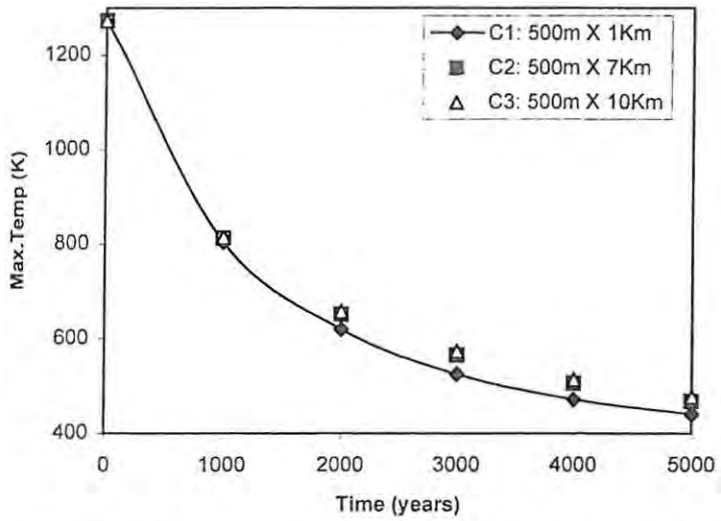

Figure 8.4: Maximum temperature vs time graph for Model C.

While cooling takes place in the magma chamber, the magma convects forming two convection cells. These convection cells can be seen in Figure 8.5. The two convection cells are moving in opposite directions with the maximum velocity at the vertical sides of the magma chamber. The flow is ascending in the middle and falling at the sides.

The convection slows down while cooling and the convection cells reduce in size until convection stops after 4000 years. By this time the magma chamber has reached a temperature of approximately 550 K.

8.1.2 The high permeability section (HPS)

The flow in the HPS is linear (meaning that no convection cells can be observed) and its maximum velocity is reached at the end of the HPS furthest from the magma chamber. Figure 8.6 illustrates the direction of the flow (see more details given in Figure 8.8).

In the first 1000 years, the velocity in the convecting magma chamber is higher than that of the flow in the HPS. At the same time, the flow in the

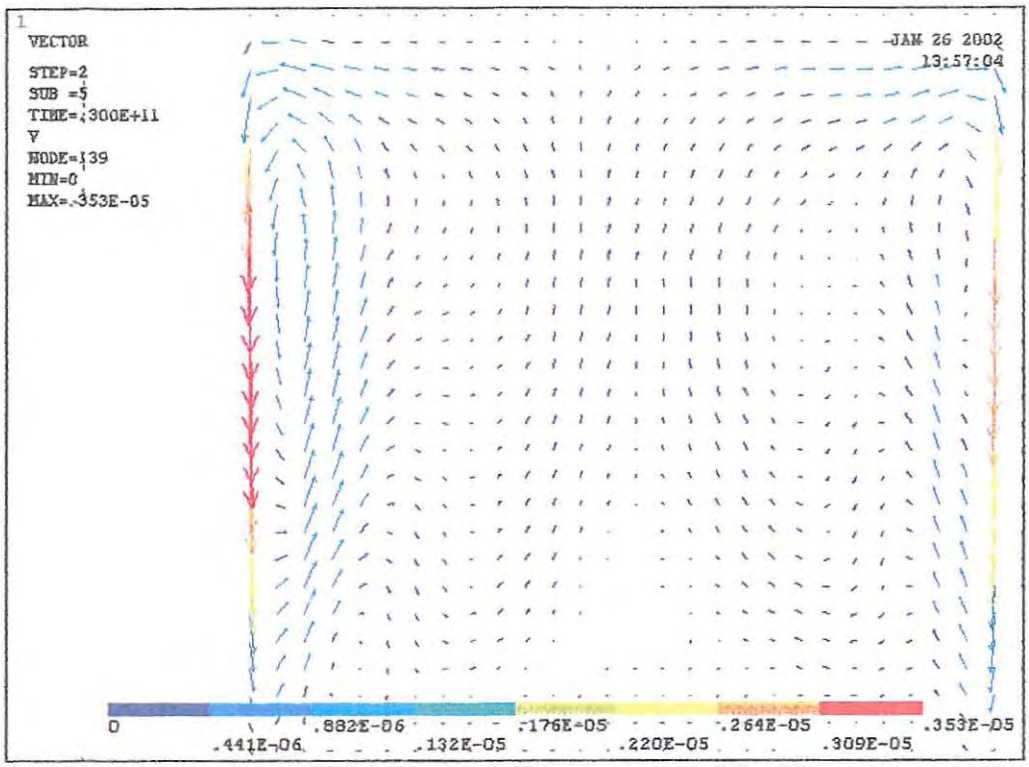

Figure 8.5: Velocity profile of the magma chamber after 1000 years, Model C2.

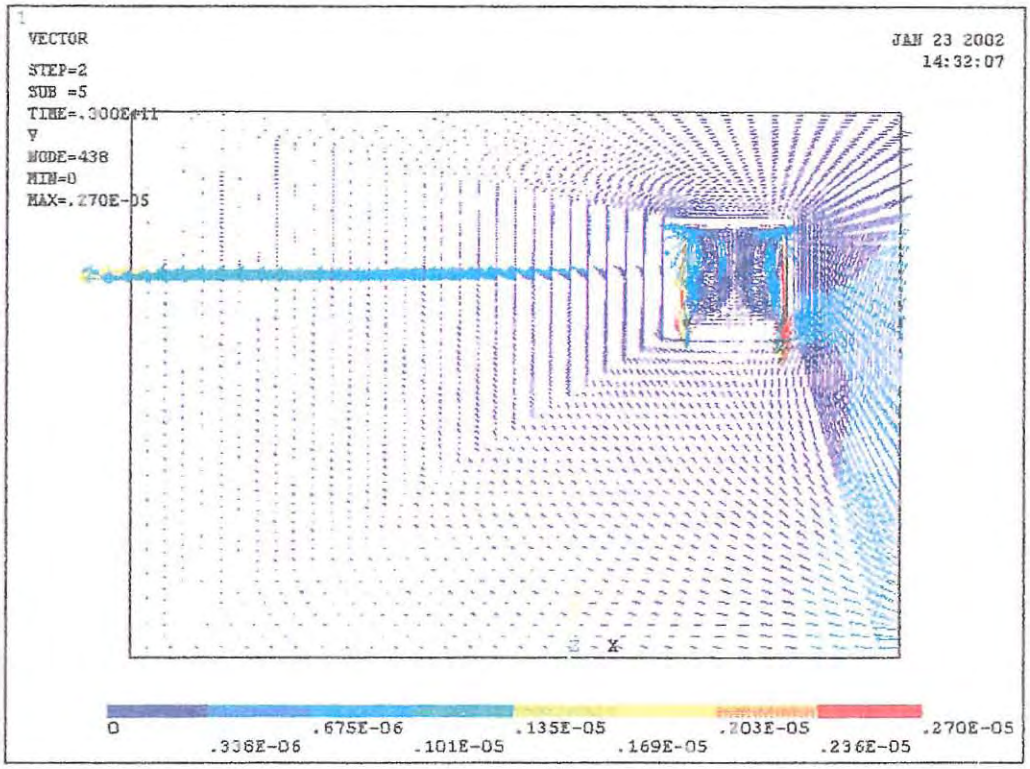

Figure 8.6: Velocity profile of the flow for Model A2 after 1000 years.

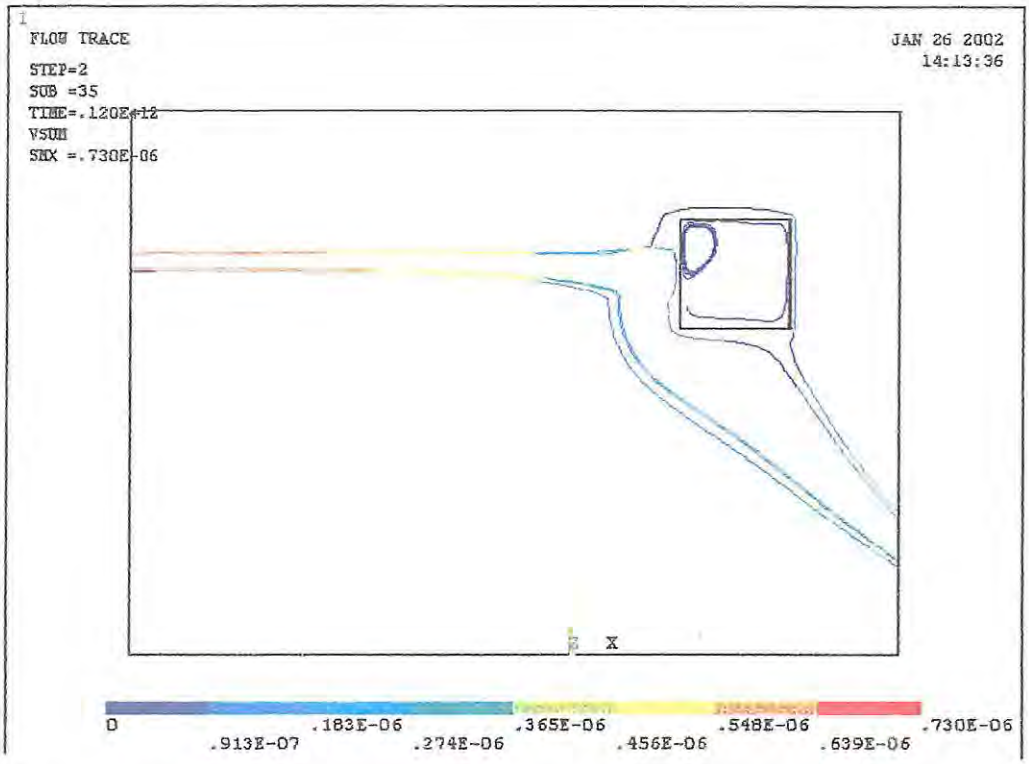

Figure 8.7: Particle path for the groundwater in the country-rock after 4000 years for Model C2.

HPS is much more vigorous than that in the rest of the country-rock. This is because there is much less hydraulic resistance to overcome in the HPS than in the country-rock.

The flow in the HPS is recharged from the rest of the country-rock. This is shown in Figure 8.7 which was produced as follows. Seven particle paths are presented. Two of them are inside the magma chamber and the rest are in the country-rock. The software has the ability to follow the paths of a finite number of particles arbitrarily chosen by the user. Figure 8.7 was chosen from a number of other 'particle path' diagrams because it illustrates best the direction of the flow.

A detailed velocity profile in the HPS in Figure 8.8 shows that on the right hand side, near the magma chamber, the direction of the flow is upwards due to the high temperatures near the magma chamber wall. As noted above, the maximum velocity is reached towards the end of the HPS. This is in

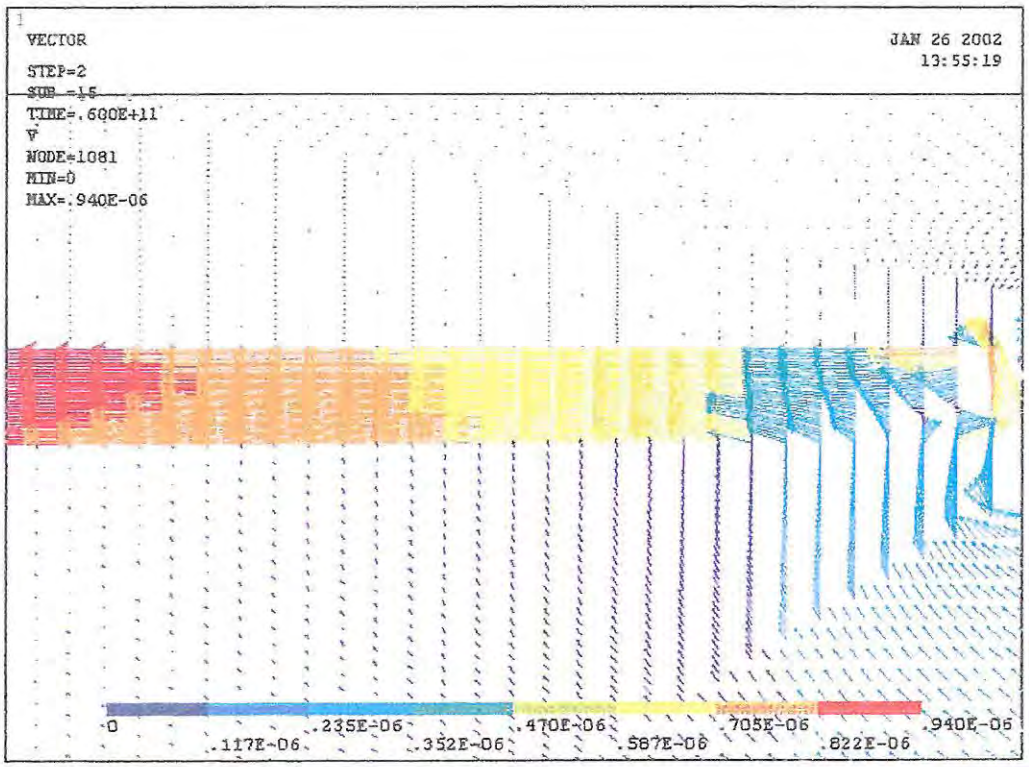

Figure 8.8: Detailed velocity profile in the HPS.

concordance with Figure 8.7 which shows the buoyancy occuring near the magma chamber.

The velocity-time graphs for Models A and C are presented in Figures 8.9 and 8.10. The readings taken at the 1000 year marks are approximate because the maximum velocity is in the magma chamber. All the other readings are exact.

8.2 The 'closed' model results

8.2.1 The magma chamber

The magma chamber cools down following the same pattern as for the 'open' models. The cooling curves for the 'closed' models (B and D—see Table 6.1) are presented in Figures 8.11 and 8.12. The magma convection pattern is

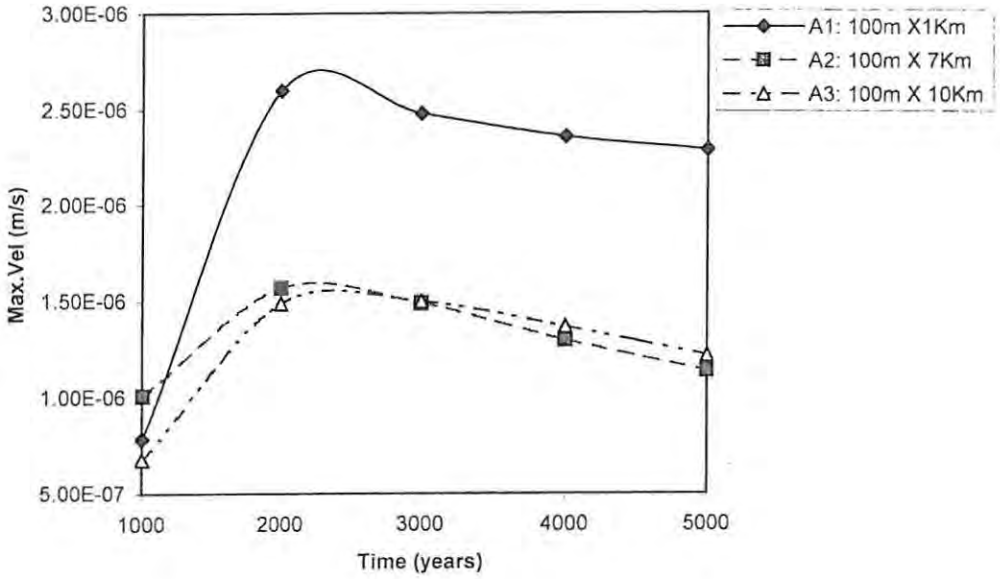

Figure 8.9: Model A: the variation of the maximum velocity in the HPS.

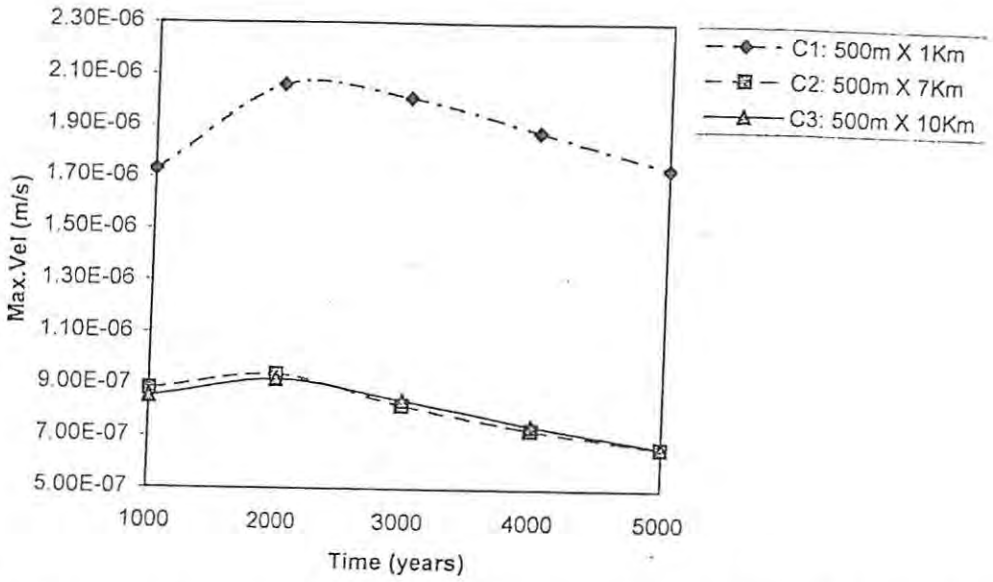

Figure 8.10: Model C: the variation of the maximum velocity in the HPS.

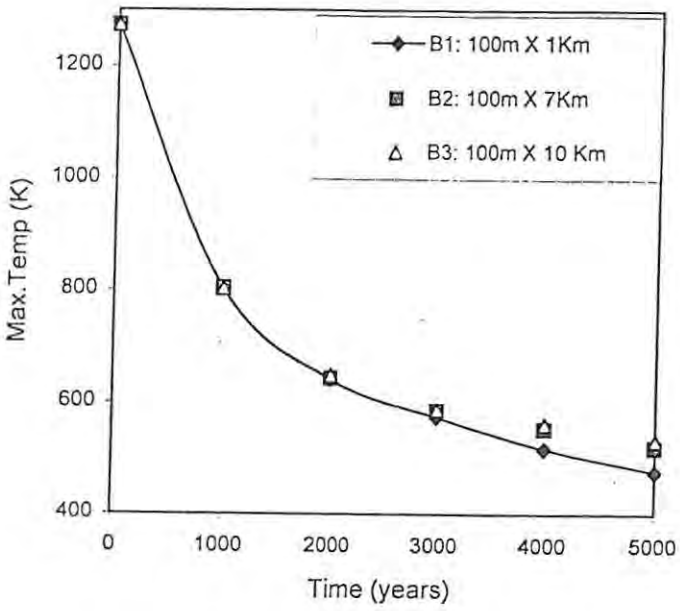

Figure 8.11: Maximum temperature vs time graph for Model B.

the same as for the 'open' models as well.

8.2.2 The high permeability section (HPS)

The flow in the HPS behaves differently from that in the 'open' models. A convection cell forms in the HPS. This convection cell can already be seen after 1000 years. Figure 8.13 shows the detail in the HPS near the magma chamber where the convection cell can be observed.

The dimensions of the convection cell are important because we believe that the ores are most likely to be deposited in the limbs of the convection cell. The width of the convection cell equals the width of the HPS, and its length is approximately 1-3 km for Model D2. This is illustrated in Figure 8.14 with a particle path diagram as used in Figure 8.7.

The magnitude of the velocities versus time for Models B and D are presented in Figures 8.15 and 8.16. The maximum velocity is reached again after

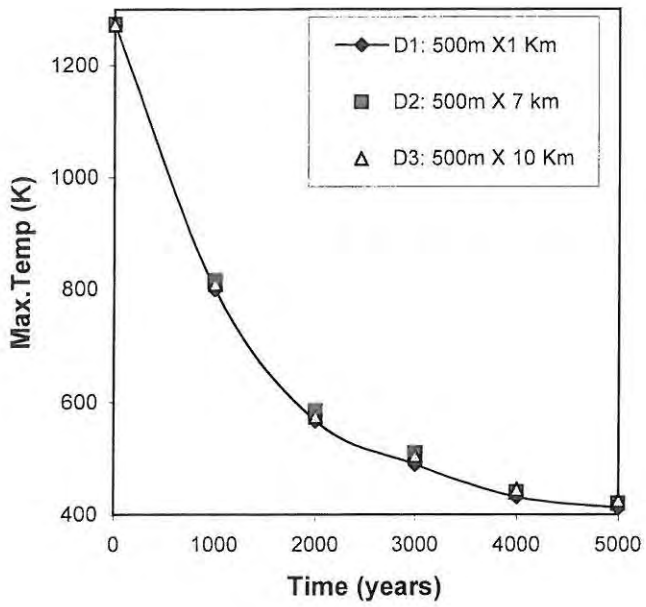

Figure 8.12: Maximum temperature vs time graph for Model D.

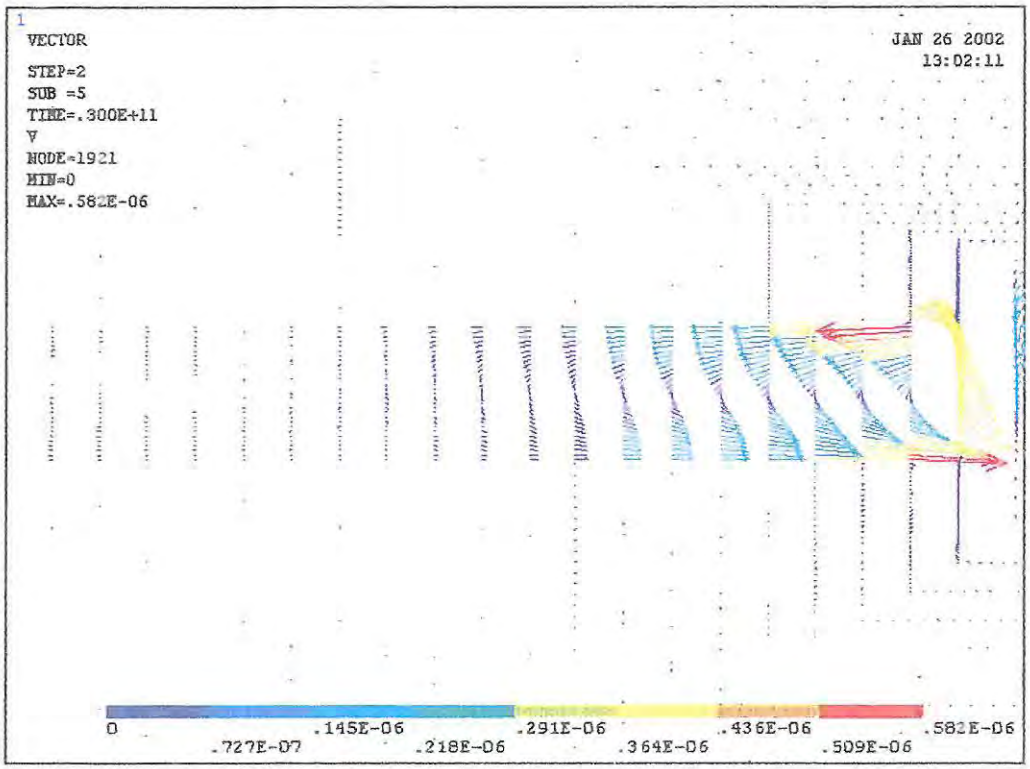

Figure 8.13: Detail in the HPS after 1000 years for Model D2.

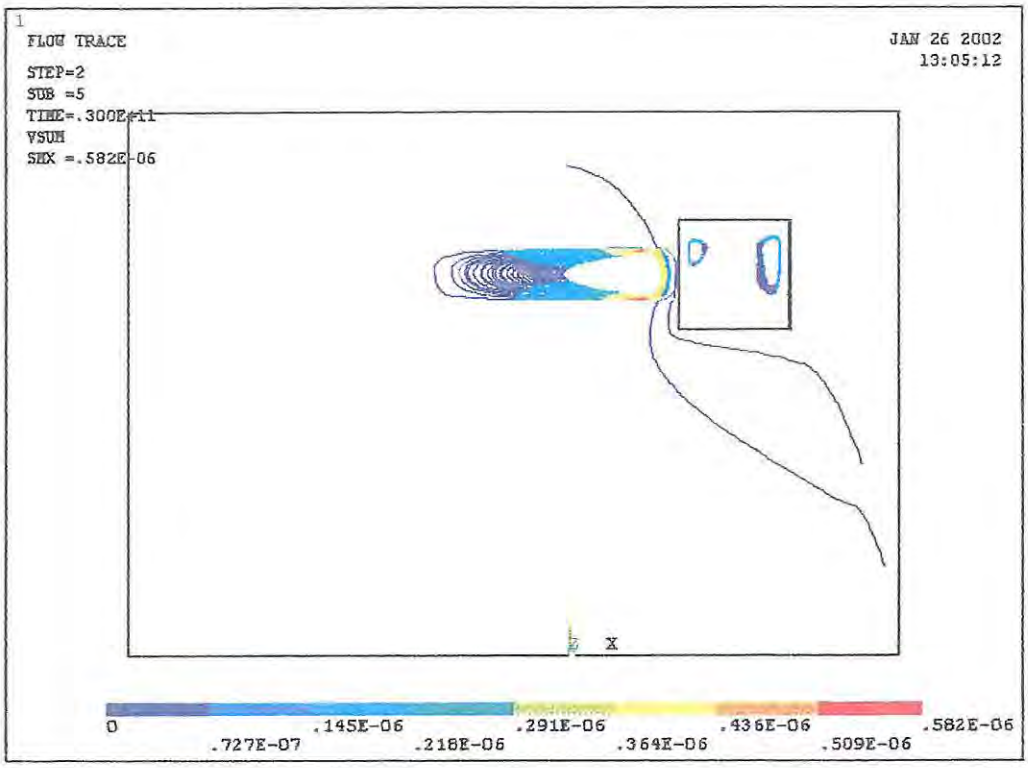

Figure 8.14: Convection cells in the HPS and in the magma chamber after 2000 years for Model D2.

2000 years and decreases thereafter. As in the case of the previous models, the 1000 year reading is approximate because the velocity of the convecting magma is greater than the maximum velocity of the flow in the HPS.

8.3 The correlation between the magma temperature and the velocity of the flow in the HPS

It is possible to develop a simple understanding of the correlation between the velocity of the flow in the HPS and the temperature of the adjacent magma. By using the terms input and output in the general modelling sense it can be observed that the input is the magma temperature and the output

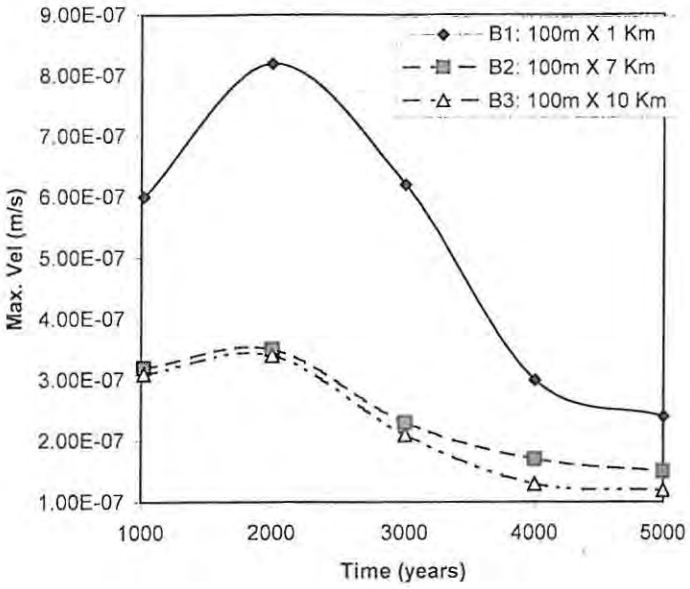

Figure 8.15: Maximum velocity in the HPS for Model B.

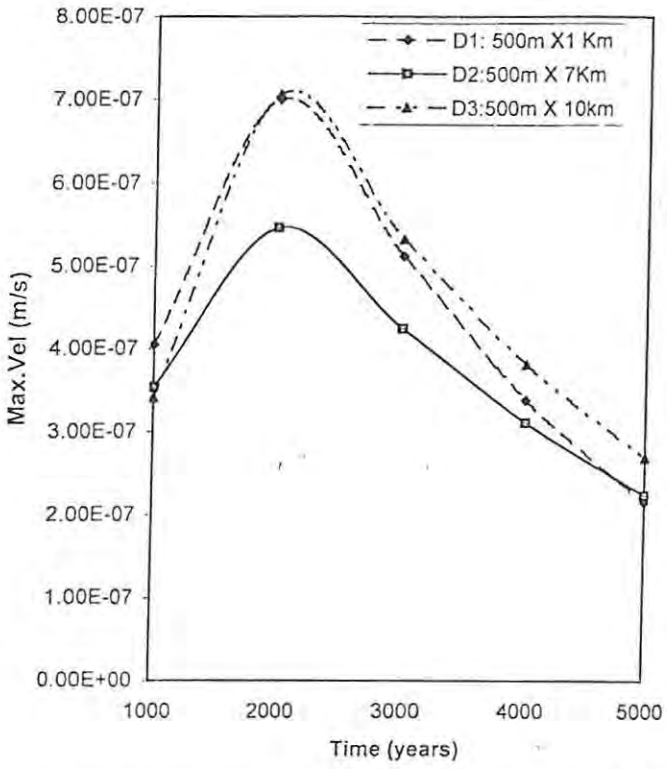

Figure 8.16: Maximum velocity in the HPS for Model D.

Initial conditions	Boundary conditions	Dimensions
T = 348K	$v_x = v_y = 0$	1 km × 100 m
at all nodes	at all exterior nodes	
	T = 1273K for right hand side nodes	
	T = 293K for top nodes	
	T = 418K for bottom nodes	

Table 8.1: Simple HPS model: boundary conditions and dimensions.

is the velocity in the HPS. Both vary with time as well. The velocity-time graph and temperature-time graph are shown in Figures 8.17 and 8.18. To find out what the correlation is, a simple model of the HPS on its own was devised. The same boundary conditions and initial conditions were applied to the simple model as were found in the 'big' model. The input temperature at the wall adjacent to the magma chamber was kept constant at 1273K (step input temperature). The dimensions and boundary conditions are given in Table 8.1

The velocity-time data for the step input temperature is presented in Figure 8.19. This is very close to an exponential function described by the equation

$$V_m = \left(1 - e^{\frac{-t}{\tau}}\right) \tag{8.1}$$

where V_m is the maximum velocity in $\mathrm{m} \cdot \mathrm{s}^{-1}$, τ is the time constant of the system and t is time in seconds. For system B1, τ = 4287 years.

Such a response to a step input is characteristic of a linear system (by

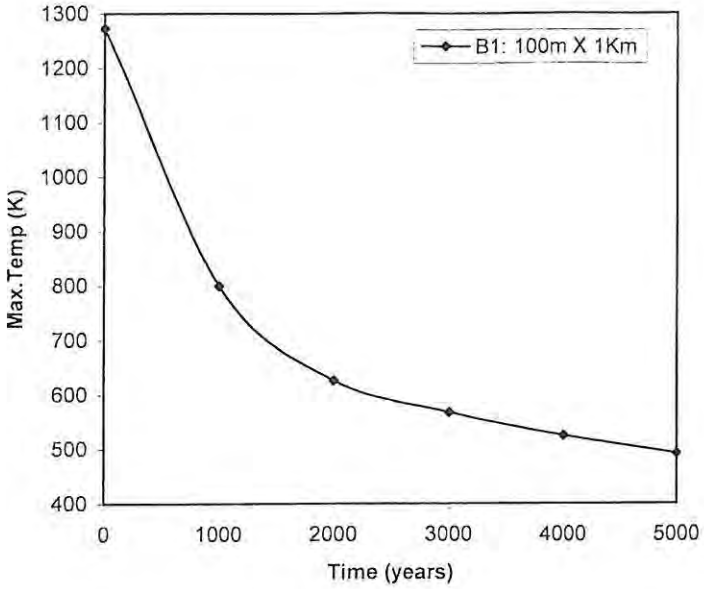

Figure 8.17: Maximum temperature vs time graph of the magma for Model B1.

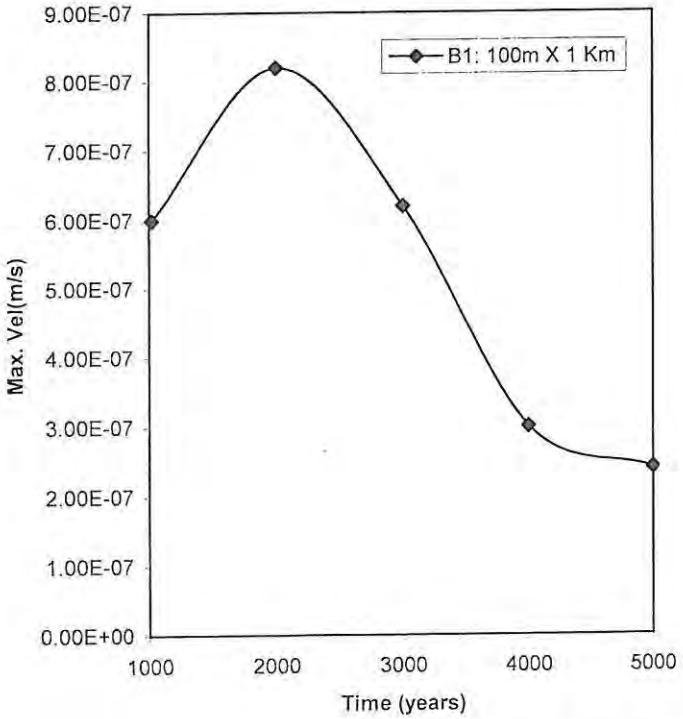

Figure 8.18: Maximum velocity vs time graph of the groundwater for Model B1.

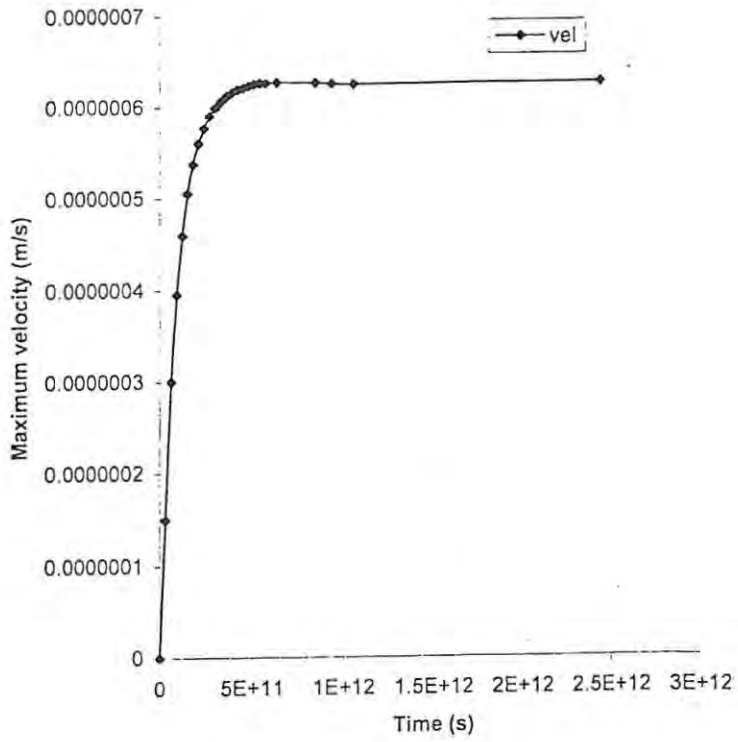

Figure 8.19: Maximum velocity vs time graph for the step input temperature.

analogy with a RC system) governed by the differential equation

$$\frac{dV}{dt} + V(t) = T \tag{8.2}$$

where T is the temperature and V is the velocity (Oppenheim, Wilsky and Young, 1983).

By changing the input temperature to

$$T(t) = T_0 e^{\frac{-t}{\Gamma}} \tag{8.3}$$

where Γ is the time constant, the differential equation becomes

$$\frac{dV}{dt} + V(t) = T(t) \tag{8.4}$$

The solution to this differential equation is

$$V(t) = e^{\frac{-t}{\tau}} - e^{\frac{-t}{\Gamma}} \tag{8.5}$$

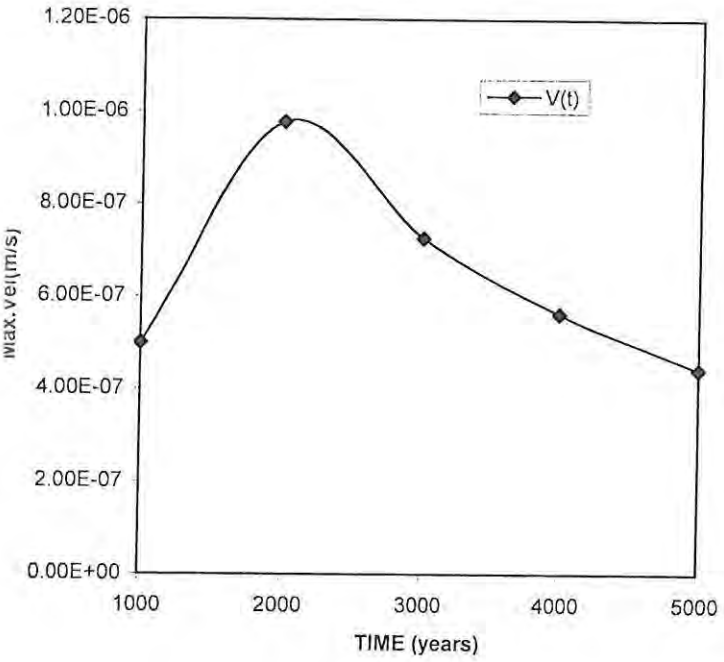

Figure 8.20: Velocity-time graph for variable input temperature.

as shown in Figure 8.20, using $\tau = 4287$ years and $\Gamma = 723$ years. The value of Γ coresponds to the exponential curve shown in Figure 8.18.

This function has a maximum at

$$t = \frac{\ln \frac{\Gamma}{\tau}}{\frac{1}{\tau} - \frac{1}{\Gamma}} \tag{8.6}$$

which gives $t = 1547$ years for the value of Γ and τ. This compares favorably with the 2000 years in Figure 8.15. This shows in broad terms how the detailed system works. The 'thermal inertia' of the 'HPS system' is characterized by τ which means that the velocities in the HPS take this amount of time to build up to 63% of their final values. However, because the magma chamber is cooling approximatelyexponentially (characterized by Γ), the velocities will eventually die down.

The combination of these two effects explains why the velocities reach a maximum and then decrease significantly as observed in the 'big models'.

Chapter 9

Conclusions

9.1 Summary of 'open' and 'closed' model results

The 'open' model gives an idea of how the groundwater flow looks in a section of higher permeability than the adjacent country-rock. The important points are that the flow is straight and that there is a recharge phenomenon in place to feed the flow in the HPS. The model with the shortest HPS cools the fastest. There are no major differences between the 100 m and 500 m widths of the HPS. For both widths used, the flow has the same pattern. The maximum velocity is reached in the HPS at the furthest end from the magma chamber. For both widths the maximum velocity is observed in the shortest HPS with no big differences for the other two lengths. For all 'open' models, the order of magnitude of the maximum velocity in the HPS is the same.

The 'closed' models reflect a number of similarities. The model with the

shortest HPS cools the fastest, for both widths of the HPS. The flow pattern in both 'closed' models is the same: a convection cell forms in the HPS and these calculations suggest that mineralization may be expected close to the magma chamber walls. The heat from the magma warms up an adjacent volume of water making it buoyant. This volume of water rises to the top of the HPS and, because the adjacent region is much less permeable than the HPS, the flow is deflected sideways. By moving along the top of the HPS, the water gives away heat to the cooler regions above. By giving away heat, it cools down until it is colder than the regions below it. The volume of water then sinks.

There is a correlation between the maximum velocity in the HPS and the temperature variation of the cooling magma chamber. This correlation is described by a differential equation. The solution to this differential equation give the time at which the maximum velocity in the HPS is reached. These results show the groundwater convecting under the heat generated by the cooling magma chamber. There is therefore the possibility that the formation of valuable mineral deposits has a hydrothermal component.

Using the models presented, there are ways of finding out where the valuable minerals are most likely to be deposited. The flow pattern shows in which direction the groundwater is likely to flow, and by looking at the temperature profiles it is easy to see where the temperatures and velocities are high enough to dissolve minerals containing valuable metals. The dissolved metals can then be traced to regions where the temperature has dropped to values low enough to cause their precipitation and deposition.

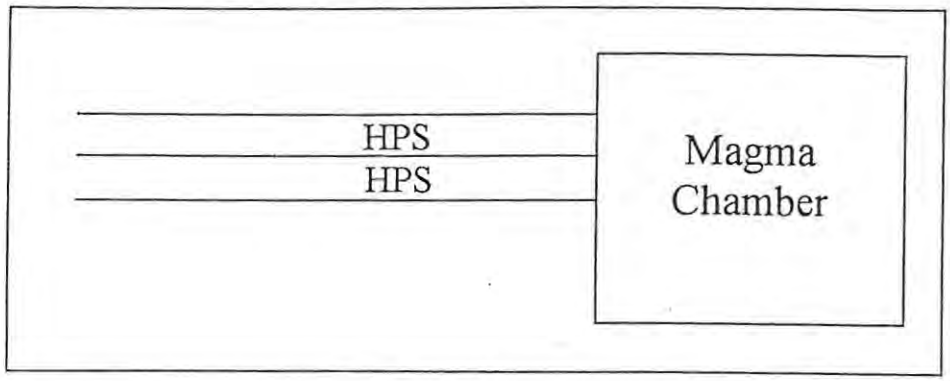

Figure 9.1: Multiple HPS

9.2 Suggestions for further research

Future models should include variations in the permeability throughout the country-rock. Another direction to follow would be to extend the dimensions of the magma chamber and the country-rock surrounding it. By increasing these dimensions, the cooling time of the magma chamber will increase and possibly the flow in the sections of higher permeability therefore will have different characteristics. Furthermore, the HPS could be positioned at different angles, (Figure 9.2), and multiple sections could be included in a simple model (Figure 9.1).

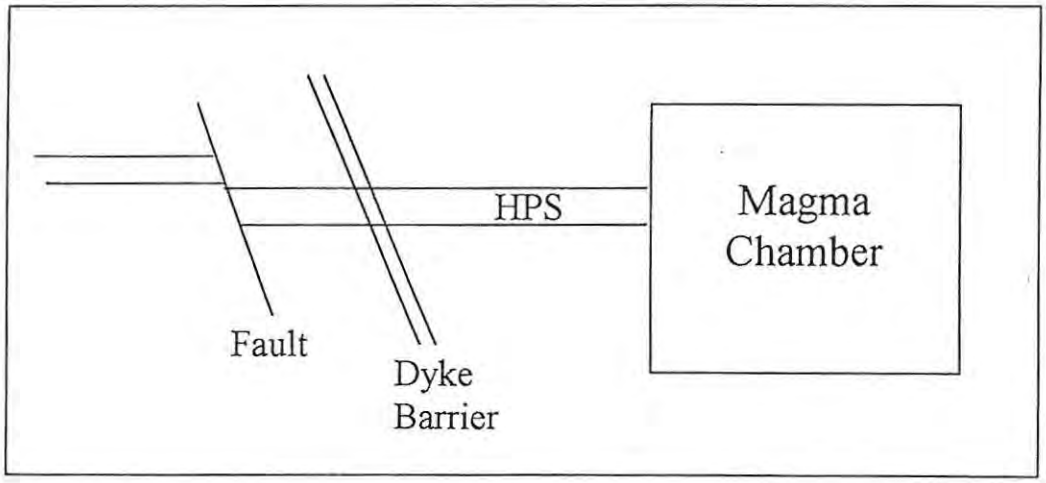

Figure 9.2: HPS positioned at different angles

Appendix A

ANSYS and FLOTRAN

This appendix contains an extract from the FLOTRAN Theoretical Manual (1992). The purpose of the appendix is to provide the reader with information about the ANSYS package.

ANSYS is a finite element analysis software package which can perform steady state and transient thermal analysis as well as static, modal, transient dynamic, spectrum, harmonic response, buckling and nonlinear analysis. There is available an electromagnetic section which offers static magnetic or transient magnetic two or three dimensional analysis as well as high frequency electromagnetic analysis, far-field electrostatic analysis and electric circuit analysis. FLOTRAN is the computational fluid dynamics component of ANSYS and it can model flow which can be laminar or turbulent, incompressible or compressible, steady-state or transient and thermal.

Most of the models in this work used ANSYS 5.5 and 5.6 version. The most recent version is ANSYS 7.0. The web site address is www.ansys.com.

A.1 Tri-diagonal matrix algorithm (TDMA) solver

TDMA is a fast, approximate solver and performs a user-specified number of iterations through the problem domain. The TDMA algorithm in FLOTRAN is a variation of the direct *Tri-Diagonal Matrix Algorithm.* This is the preferred method used for this model because of the shorter computing time required compared with other two methods.

The TDMA solver is used for non-symmetric systems. The idea is to introduce all entries, which are not sub- or super-diagonal elements, as additional source terms.

The FLOTRAN TDMA algorithm approximates the algebraic equations as :

$$A_i X_{i-1} + B_i X_i + C_i X_{i+1} = D_i \tag{A.1}$$

where

$$A_i = a_{ii-1} \tag{A.2}$$

$$B_i = a_{ii} \tag{A.3}$$

$$C_i = a_{ii+1} \tag{A.4}$$

$$D_i = S_i - \sum_{j=1}^{N} a_{ij} X_j, \qquad j \neq i-1, i, i+1 \tag{A.5}$$

The algorithm uses *Gaussian elimination* without pivoting as follows :

$$B_i = B_i - \left(\frac{A_{i-1}}{B_{i-1}}\right) C_{i-1} \tag{A.6}$$

$$D_i = D_i - \left(\frac{A_{i-1}}{B_{i-1}}\right) D_{i-1} \tag{A.7}$$

The back substitution becomes :

$$X_i = \frac{(D_i - C_i X_{i+1}}{B_i}, \qquad i = N-1, N-2, ..., 1 \tag{A.8}$$

Two items to note about this TDMA algorithm :

- for an unstructured mesh (no sub- or super-diagonals), it becomes equivalent to *Gauss-Seidel*;
- the algorithm is *not* direct since it iterates on X for a user-specified number of sweeps.

A.2 Techniques to improve numerical stability

The term 'numerical stability' is used with reference to the discretization of the non-linear advection terms in the governing equations. It is noted that some form of upwinding is required in this discretization to minimize the occurences of dispersion errors which appear as spatial oscillations in the solution variable. Upwinding is then a numerical tool used to stabilize the solution of the unwieldy non-linear terms. Numerical stability also refers to the tendency for the solution of a system to converge. A system is unstable if it is inclined to diverge and it is often characterized by a poorly conditioned coefficient matrix or one that is not positive definite. Two techniques exist in FLOTRAN to improve conditioning by making the coefficient matrix more diagonally dominant without changing the system mathematically. These are particularly useful in problems having non-symmetric matrices.

In these cases, the effects of poor conditioning can be dramatic (FLOTRAN Theoretical Manual, 1992).

The three techniques mentioned are: inertial relaxation, solution relaxation (no detail is given because there was no need to use this technique) and the introduction of the artificial viscosity term.

A.2.1 Artificial viscosity

An artificial viscosity term has been included in the momentum equation to assist in the solution of problems that have particularly high spatial gradients in the solution variable,as for the case of shocks and expansion fans in compressible flows. Like the inertial relaxation, this too is a means of improving diagonal dominance in the coefficient matrix. The name artificial viscosity is derived from the fact that its inclusion is a departure from the true Navier-Stokes equations and it is diffusive in the same fashion as viscosity. The artificial viscosity q is incorporated with the pressure gradient term in the momentum equations :

$$\begin{aligned} -\frac{\partial P}{\partial x} &\rightarrow -\frac{\partial}{\partial x}(P+q) \\ -\frac{\partial P}{\partial y} &\rightarrow -\frac{\partial}{\partial y}(P+q) \\ -\frac{\partial P}{\partial z} &\rightarrow -\frac{\partial}{\partial z}(P+q) \end{aligned} \tag{A.9}$$

where

$$q = -(\lambda + 2\mu)\left[\frac{\partial u}{\partial x} + \frac{\partial v}{\partial y} + \frac{\partial w}{\partial z}\right]. \tag{A.10}$$

When Equation (A.10) is substituted into (A.9), second derivative diffusion terms arise that are similar in form to the dilatation terms in the Navier-Stokes equations.

FLOTRAN uses an adjustable coefficient ($ArtVis$) in the place of $(\lambda+2\mu)$. The artificial viscosity terms in FLOTRAN are then :

$$\begin{aligned}
-\frac{\partial}{\partial x}(P+q) &\rightarrow -\frac{\partial P}{\partial x} + \text{ArtVis}^*\frac{\partial}{\partial x}\left(\frac{\partial u}{\partial x}+\frac{\partial v}{\partial y}+\frac{\partial w}{\partial z}\right) \\
-\frac{\partial}{\partial y}(P+q) &\rightarrow -\frac{\partial P}{\partial y} + \text{ArtVis}^*\frac{\partial}{\partial x}\left(\frac{\partial u}{\partial x}+\frac{\partial v}{\partial y}+\frac{\partial w}{\partial z}\right) \\
-\frac{\partial}{\partial z}(P+q) &\rightarrow -\frac{\partial P}{\partial z} + \text{ArtVis}^*\frac{\partial}{\partial x}\left(\frac{\partial u}{\partial x}+\frac{\partial v}{\partial y}+\frac{\partial w}{\partial z}\right). \qquad \text{(A.11)}
\end{aligned}$$

The artificial viscosity terms in (A.11) are discretized using *Galerkin's weighted integral method*, just as for the diffusion terms in the generalized scalar transport equation (5.1) (FLOTRAN Theoretical Manual, 1992). Artificial viscosity is purely a numerical tool and should be used only as such. Adding the artificial viscosity does not compromise the accuracy of the solution (FLOTRAN Theoretical Manual, 1992). Artificial viscosity smooths the velocity solution in regions of steep gradients. It has proven useful in aiding convergence of compressible problems and in smoothing velocity solutions in incompressible problems with distributed resistance (ANSYS CFD FLOTRAN Analysis Guide, 1994).

A.3 FLOTRAN thermal analysis

In a thermal analysis, the temperature equation is solved to determine temperature. Even if temperature itself is not important, the variation of fluid properties with temperature may be important enough to warrant a thermal analysis. In addition to calculating a temperature field, a thermal analysis provides heat fluxes at problem boundaries and heat transfer coefficients

based on an assumed bulk or ambient temperature (ANSYS CFD FLOTRAN Analysis Guide, 1994).

A.4 FLOTRAN transient analysis

The transient analysis algorithm is activated by setting the transient solution option. Because the algorithm is implicit in nature, no stability restrictions exist on the time step size. FLOTRAN must execute global iterations to converge within a time step. The time step terminates when either of the following happens:

- The convergence criteria are met
- The maximum number of global iterations allowed per time step executes.

As soon as the convergence monitor criteria are met, the time step terminates. The time step terminates on the number of global iterations allowed if the convergence monitor criteria are not met (ANSYS CFD FLOTRAN Analysis Guide, 1994).

A.5 The FLOTRAN fluid element

The element FLOTRAN 141 (2D) (see Figure A.1) is used to model transient or steady-state fluid/thermal systems that involve fluid and/or non-fluid regions. The conservation equations for viscous fluid flow and energy are solved in the fluid region, while only the energy equation is solved in the non-fluid region. For the CFD FLOTRAN elements the velocities are obtained from the

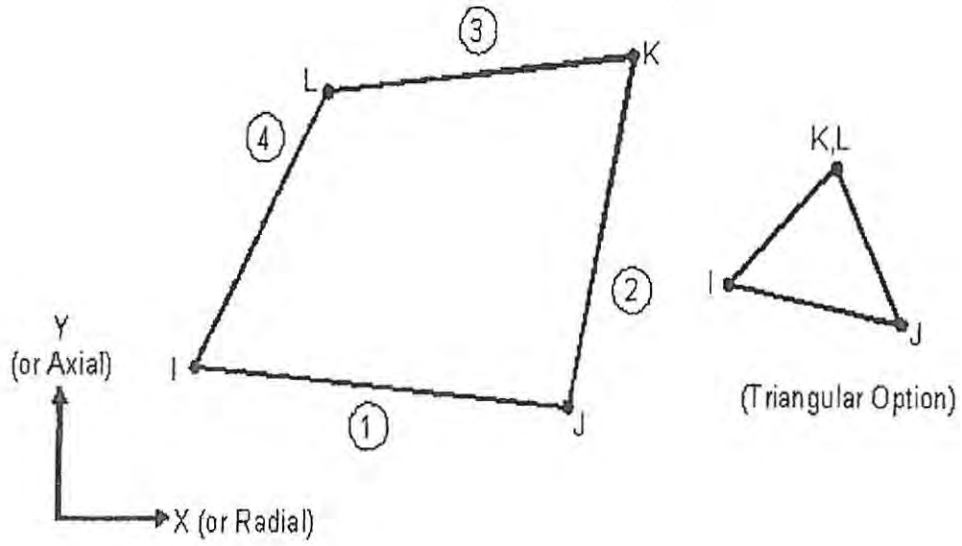

Figure A.1: Quadrilateral or triangular element geometry (from ANSYS Elements Reference, 1994)

conservation of momentum principle and the pressure is obtained from the conservation of mass principle. The temperature is obtained from the law of conservation of energy. A segregated sequential solver algorithm is used, that is, the matrix system derived from the finite element discretization of the governing equation for each degree of freedom is solved separately. The flow problem is nonlinear and the governing equations are coupled together. The sequential solution of all the governing equations, combined with the update of any temperature or pressure dependent properties, constitutes a global iteration. The number of global iterations required to achieve a converged solution may vary considerably, depending on the size and stability of the problem. Transport equations are solved for the mass fractions of up to six species.

If the material number of a FLUID 141 element is 1, it is assumed to be a fluid element. Its properties (density,viscosity, thermal conductivity and specific heat) are defined with a series of FLDATA commands.Thermal conductivity and specific heat are relevant and necessary only if the problem is thermal in nature. The properties can be a function of temperature through relationships specified by the FLDATA, PROT command. In addition the density may vary with pressure (per ideal gas law) if the fluid is specified to be air or a gas (ANSYS Elements Reference, 1994).

A.6 Global iterations

A FLOTRAN analysis is nonlinear and uses a sequential solution, so the first thing to do is to decide how many global iterations should be executed. A global iteration is the solution, in sequence, of all relevant governing equations

followed by any fluid property that are needed. In a transient simulation, a time loop exists around the global iteration loop. During a global iteration, ANSYS/FLOTRAN obtains approximate solutions to the momentum equations and uses them as forcing functions to solve a pressure equation based on conservation of mass. ANSYS uses the resulting pressures to update the velocities so that the velocity field conserves mass. At request, the ANSYS program solves the temperature equation and updates temperature dependent properties.

A.7 Convergence monitors

As a FLOTRAN simulation proceeds, ANSYS calculates convergence monitors for each degree of freedom every global iteration. Convergence monitors are computed for velocities (VX, VY, VZ), pressure (PRES), temperature (TEMP), turbulent kinetic energy (ENKE), kinetic energy dissipation rate (ENDS), and any active species transport equation (SPO1-SPO6).

The convergence monitors are a normalized measure of the solution's rate of change from iteration to iteration. Denoting by the general field variable, Φ, any DOF, the convergence monitor is defined as follows :

$$\text{ConvMon} = \frac{\sum_{i=1}^{N} \left| \Phi_i^k - \Phi_i^{k-1} \right|}{\sum_{i=1}^{N} \left| \Phi_i^k \right|} \tag{A.12}$$

The convergence monitor represents the sum of changes of the variable calculated from the results between the current k^{th} iteration and the previous $(k-1)^{th}$ iteration, divided by the sum of the current values. The summation

is performed over all n nodes, using the absolute values for the differences.

A.8 The distributed resistance

A distributed resistance provides a convenient way to approximate the effect of porous media without actually modelling the geometry of those features. It is artificially imposed, unrecoverable loss associated with geometry not explicitly modelled. Any fluid element with a distributed resistance will have a real constant set number greater then 1 assigned to it. The resistance to flow, modeled as a distributed resistance, may be due to one or a combination of these factors: a localized head loss (K), a friction factor (f), or permeability (C). The total pressure gradient is the sum of these three terms, as shown below for the X direction.

$$\frac{\partial p}{\partial X_r} = -\left(K\rho V_x|V| + \frac{f}{D_h}\rho V_x|V| + C\mu V_x\right) \qquad \text{(A.13)}$$

where

X_r = $X_{\text{resistance}}$

ρ = is the density (mass $\cdot$ length^{-3})

μ = viscosity (mass $\cdot$ length^{-1} $\cdot$ time)

RE = is the local value of the Reynolds Number (calculated by the program)

$RE = \dfrac{\rho V D_h}{\mu}$

f = is the friction coefficient (calculated by the program) $f = aRE^{-b}$.

A.9 Multiple species option

Several fluids, each with different properties, are tracked if the multiple species option is invoked (FLADATA,SOLU,SPEC,TRUE).

A single momentum equation is solved for the flow field. The properties for this equation are calculated from those of the species fluids and their respective mass fractions if the user specifies the composite gas option (FLDATA, PROT, DENS, CGAS)for density or the composite mixture option(FLDATA, PROPT, DENS, CMIX). CGAS only applies for density, but CMIX applies to density, viscosity or conductivity. If these options are not invoked, the species fluids are carried by a bulk fluid, with the momentum equation solved with properties of a single fluid.

Appendix B

Steps in building up a model

This appendix provides the detailed steps followed in building up a typical model in ANSYS.

- Select the disciplines needed to solve the problem, in this case, THERMAL and CFD FLOTRAN.
- Select the appropriate element to be used in the finite element procedure. The element chosen is FLUID 141 which can support fluid material properties as well as solid material properties.
- Introduce the material properties and the set of real constants.
- Plot the key points, lines and areas which describe the geometry of the model.
- Attribute the different materials to their respective areas.
- Mesh. Use mapped meshing.
- Fluid properties are given using the Multiple Species option.

- Initial conditions should be applied:
  - all nodes contained in the magma chamber start by having a temperature of 1273 K. The same nodes are given a mass fraction of '1' for all magmatic fluid physical properties and a mass fraction of '0' for all groundwater physical properties. By doing this, I make sure that the magma chamber has the magmatic fluid properties attributed to it.
  - to all nodes belonging to the country-rock area the appropriate initial temperature should be given, as well as a mass fraction of '1' for all groundwater physical properties and a mass fraction of '0' for all magmatic fluid properties. This is to make sure that only groundwater physical properties were attributed to those areas.
- Boundary conditions
  - to all magma chamber exterior nodes a zero velocity in both the X and Y direction was applied (the non-slip boundary condition).
  - the same zero velocity in both X and Y direction was applied to all top line exterior nodes.
  - a temperature of 293 K was applied on the top line exterior nodes.
  - a temperature of 398 K was applied to all bottom line nodes (replicating the geothermal gradient)
  - $g = 9.81 \quad \mathrm{m \cdot s^{-2}}$
  - artificial viscosity (to improve the numerical stability)
  - set the solution options

- set the execution controls
- solve the problem
- read the results
- plot the temperature solution
- plot the velocity solution

Appendix C

Glossary of geological terms

Andesite magma : magma with a SiO_2 content between 50% and 70%.

Dacite : a fine-grained extrusive rock with the same general composition as andesite but having less calcic feldspar.

Felsic or granitic magma : magma with 70% SiO_2

Igneous rock : rock formed by the solidification of magma.

Magma : a complete or partly molten natural substance, which, on cooling, solidifies as a crystalline or glossy igneous rock.

Mafic or basaltic magma : magma with only about 50% SiO_2 content

Melt : a liquid fused rock.

Orthosilicate : a salt of the hypothetical orthosilicic acid, H_4SiO_4 .

Phenocrysts : relatively large, conspicuous crystal in a porphyritic rock.

Porphyritic : a textural term for those igneous rocks in which larger crystals are set in a finer groundmass which may be crystalline or glassy, or both.

Rhyolite : the extrusive equivalent of a granite.

Silica : silicon dioxide, SiO_2.

References

J. BEAR, *Dynamics of Fluids in Porous Media*, Dover, New York, 1972.

R. BOLTZ, G. TUVE, *Handbook of Tables for Applied Engineering Science*, 1973

A.E. BOTHA, *Towards Modelling the Formation of Ore Bodies : initial results dealing with the fluid mechanical aspects of magma chamber convection*, MSc Thesis, Rhodes University, 1999.

P.L. DEVRIES, *A First Course in Computational Physics*, J. Wiley, New York, 1994.

K. HARRISON, *Finite Element Modelling of Magma Convection and Attendant Groundwater Flow*, MSc Thesis, Rhodes University, 1998.

A.R. MCBIRNEY AND T. MURASE, Rheological properties of magmas, *Ann. Rev. Earth Planet. Sci.* **12**(1984), 337-357.

L.M. MBANDEZI, *Finite element simulations of shear aggregation as a mechanism to form platinum group elements (PGEs) in dyke-like ore bodies*, MSc Thesis, Rhodes University, 2001.

T. MURASE AND A.R. MCBIRNEY, Properties of some common igneous rock and their melts at high temperature, *Geological Society of America Bulletin* **84**(1973), 3563-3592.

A.V. OPPENHEIM, A.S. WILSKY AND I.T.YOUNG, Signals and systems, 1983.

A. RICE, J.M. MOORE, S. VAN WYK, C. REMSING, *Finite element modelling of 3D free-surface kamatiite lava flows, magma circulation in sills and hydrothermal circulation driven by cooling magma chambers. Towards the understanding the role of fluid flow on the emplacement of ore deposits*, Exploration Geodynamics Conference, Western Australia, 2001.

G.R. ROBSON, Thickness of Etnean lavas, *Nature* **216**(1967), 251-252.

N. ROGERS AND C. HAWKESWORTH, Composition of Magmas, in *Encyclopedia of Volcanoes*, Academic Press, New York, 2000.

R. TYLER AND N. TYLER, Stratigraphic and structural controls on gold mineralization in the pilgrim's Rest gold field, eastern Transvaal, South Africa, *Precambrian Research* **79**(1996), 141-169.

P. WALLACE AND A.T. ANDERSON, JR., Volatiles in Magma, in *Encyclopedia of Volcanoes*, Academic Press, New York, 2000.

H.F. WANG AND M.P. ANDERSON, *Introduction to Groundwater Modeling. Finite Difference and Finite Element Methods*, W.H. Freeman, San Francisco, 1982.

F.M. WHITE, *Viscous Fluid Flow* (Second edition), McGraw-Hill, New York, 1991.

H. WILLIAMS AND A.R. MCBIRNEY, *Volcanology*, Freeman, Cooper & Co., San Francisco, 1979.

FLOTRAN : Theoretical Manual, Compuflo, Houston, PA, 1992.

ANSYS CFD FLOTRAN : Analysis Guide, Swanson Analysis Systems, Houston, PA, (Release 5.3) 1994.

ANSYS : Advanced FLOTRAN, Swanson Analysis Systems, Houston, PA, 1994

ANSYS : Elements Reference, Swanson Analysis Systems, Houston, PA, 1994.